DESIGN AND FABRICATION OF A HIGH-TEMPERATURE HIGH-VACUUM FURNACE TO HEAT TREAT NIOBIUM FOR SUPERCONDUCTING RADIO FREQUENCY CAVITIES

By

Saravan Kumar Chandrasekaran

A THESIS

Submitted to
Michigan State University
in partial fulfillment of the requirements
for the degree of

MASTER OF SCIENCE

Mechanical Engineering

2010

ProQuest LLC
789 East Eisenhower Parkway
P.O. Box 1346
Ann Arbor, MI 48106-1346

ABSTRACT

DESIGN AND FABRICATION OF A HIGH-TEMPERATURE HIGH-VACUUM FURNACE TO HEAT TREAT NIOBIUM FOR SUPERCONDUCTING RADIO FREQUENCY CAVITIES

By

Saravan Kumar Chandrasekaran

The noble metal niobium is increasingly used for the fabrication of superconducting radio frequency (SRF) cavities, which accelerate charged atomic and sub-atomic particles to speeds between 5 and 100 % of the speed of light. The fabrication of SRF cavities typically involves large deformation of niobium sheet, introducing large strain in the metal. Strain produces dislocations in the metal, which is known to degrade the heat transfer properties of the metal. For improved thermal performance, annealing at 600 °C to 800 °C in vacuum can be done to stress relieve the deformed metal.

With high energy physics research aiming at higher accelerating gradients for larger particle accelerators, like the International Linear Collider (ILC), high purity niobium is desired for its improved thermal performance. One of the well known methods of increasing the purity of niobium is to heat treat the metal at temperatures between 1200 °C and 1500 °C, in vacuum and with a coating of a getter, like titanium or yttrium.

To advance the research capabilities of the SRF cavity group at the National Superconducting Cyclotron Laboratory at Michigan State University, a high-temperature high-vacuum heat treating furnace was designed and constructed for heat treating niobium samples used for materials and heat transfer research. A prototype furnace was also constructed to demonstrate novel technologies in a cost effective manner. The scale of the prototype and the sample heat treating furnace was such that most of the required equipment were available in-house. A furnace to heat treat full-size cavities can be fabricated by scaling the design of the sample heat treatment furnace.

In fond memory of N. Sharavana

ACKNOWLEDGMENT

I owe my deepest gratitude to my adviser, Dr. Neil Wright, for guidance, encouragement and valuable support through this thesis. I truly appreciate his friendliness, and for allowing me the room to do research in my own way. I am also grateful to Dr. Terry Grimm during his tenure with NSCL (currently founder of Niowave Inc.) for providing me with the opportunity to perform research at NSCL.

I would like to thank Dr. Tom Bieler and Chris Compton for all of their support through this project. I am indebted to Steve Bricker and John Bierwagen for continued unrelenting technical support and for the many useful discussions during fabrication and assembly of the furnaces. I would like to thank Dan Pendell and Tim Kole for all of the welding they performed for the furnaces. I am also grateful to Jon Wlodarczak and Dave Norton for helping me with the data acquisition and control systems for the furnaces. I would like to thank Dr. Dave Sanderson, John Yurkon, Scott Hitchcock, Jay Pline, Kelly Davidson, Kurt Kranz, Andy Thulin, Chuck Gaus and Kim Gwinn for providing valuable advice and support during fabrication and assembly of the furnace. I am also grateful to Derek Baars for helping me cut the ceramic tubes for the furnaces.

I would like to show my gratitude to my committee members, Dr. Craig Somerton and Dr. Walter Hartung, for fruitful discussions and valuable advice through the length of the thesis project.

I am also grateful to all NSCL and Mechanical Engineering staff, especially Aida Montalvo for all the support through the years. I would also like to thank my fellow graduate students at NSCL and Mechanical Engineering for all the useful conversations.

I would like to thank my family, especially my parents, Mr. L.M. Chandrasekaran and Mrs. Devi Chandrasekaran, and sister, Gayathri Chandrasekaran, for continued emotional support throughout my stay away from home. I would also like to thank

my best friend and fiancée, Deebika Balu, for all the encouragement and patience during the fabrication and testing of the furnaces, and for understanding the long, odd hours I spent working.

TABLE OF CONTENTS

LIST OF TABLES

LIST OF FIGURES

Images in this thesis are presented in color

Chapter 1

Introduction

This thesis describes the design and fabrication of a furnace to heat treat high purity niobium at temperatures ranging from 100 °C to 1250 °C. The furnace is constructed using tungsten for the heating element and molybdenum for radiation shields. The furnace is sized to accommodate niobium samples used in heat transfer and materials science research. The furnace is composed of four systems, namely, electrical, thermal shielding, vacuum, and thermometry, as is a prototype furnace that is also constructed to demonstrate the design. The prototype provided insight into the technologies required for a vacuum furnace, and offered insurance of the stability of the design analysis.

Chapter 2 provides some background on niobium cavities for particle accelerators, including a brief description of cavity fabrication methods. A justification for niobium heat treatment is provided, and the benefits for cavity performance are mentioned. Chapter 3 describes the various components of the prototype furnace and their fabrication. Calculations were performed and compared with the results from operating the prototype furnace. A furnace to heat treat niobium samples for heat transfer and materials science research was fabricated, with some shared components from the prototype furnace. Chapter 4 describes the fabrication of the different components of

the sample treating furnace. Results from operating the furnace are compared with calculations of the heat loss and power requirement of the furnace.

Chapter 2

Background

Particle accelerators are used to produce beams of charged particles of varying energies for high energy physics research, low-to-medium energy nuclear physics research, bio-medical research, medical treatment, and other applications. An important component in many particle accelerators is the *superconducting radio frequency* (SRF) cavity, which imparts energy to the charged particles via an oscillating RF field. Operating in the superconducting regime provides increased performance and overall system energy savings. The SRF cavity resonates between 50 MHz and 3000 MHz depending on the type of accelerator. In the past few decades, niobium has become the metal of choice for constructing SRF cavities, because of its high critical temperature for superconductivity ($T_c = 9.25$ K) and its ductility, which makes it easier to fabricate into cavities.

Typical cavities for high energy beams have elliptical "pill-box" shapes and can have one or more cells, depending on the operational requirements. A sectional view of a typical single cell elliptical cavity is shown in Figure 2.1.

The purity of the niobium is correlated with the *residual resistivity ratio* (RRR), which is defined as

$$\mathrm{RRR} = \frac{\rho_{e,300}}{\rho_{e,4.2}} \tag{2.1}$$

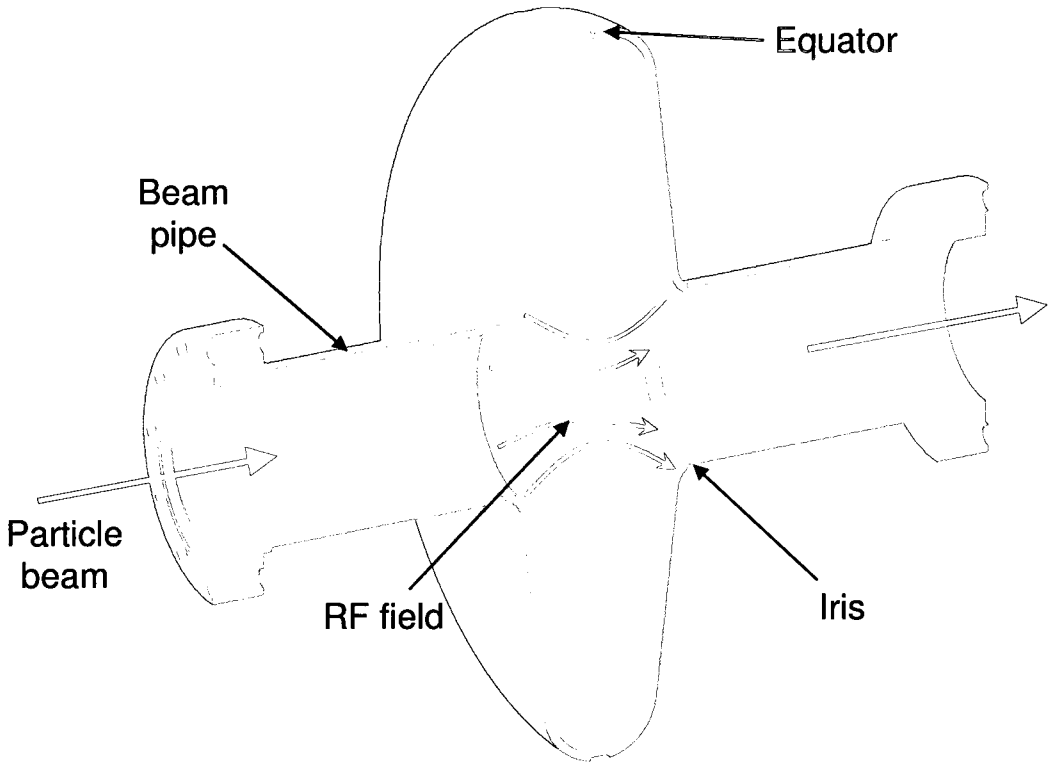

Figure 2.1: Isometric sectional drawing of a single-cell elliptical SRF cavity. Charged particles are accelerated in a vacuum by an RF field confined to the inner volume. The cavity is submerged in liquid helium.

where $\rho_{e,300}$ is the electrical resistivity at 300 K, and $\rho_{e,4.2}$ the normal-state electrical resistivity at 4.2 K.

2.1 SRF Cavity Fabrication

SRF cavities are fabricated either from rolled sheets of niobium or from niobium discs cut from ingots. Niobium ingots are produced by melting the niobium ore using an electron beam and solidifying the molten niobium into cylinders of improved purity. The RRR of the niobium is improved by melting and re-solidifying the ingot several times in a high vacuum environment. In recent years, with increased research from the SRF community and niobium vendors, niobium sheets and discs of 99.98 % purity have been produced readily. Both sheet and disc niobium undergo the same fabrication steps to produce cavities. For elliptical cavities, the main steps include stamping of the niobium using metal dies (usually made of aluminum) to get the desired shape of a half-cell, and electron beam welding of the half cells to produce the cavity.

Beam tubes and other miscellaneous parts are welded last onto the structure. Extreme care is taken to preserve surface smoothness and bulk properties during and

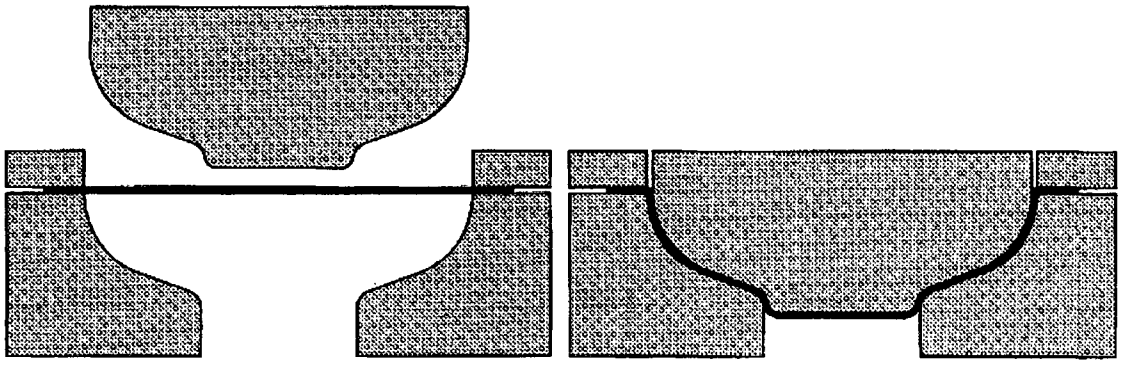

Figure 2.2: Deep drawing a niobium disk into a half cell [1].

after welding. Smoothness of the surface is important for the RF performance, while bulk properties are important for the transfer of heat from the inside surface of the cavity to the outer liquid helium bath [1].

2.2 Heat Treatment of Niobium

Stamping of niobium sheets and discs to produce the half cells introduces strain and dislocations into the niobium. Excessive dislocations can have an adverse effect on mechanical and electrical properties of the metal. Vacuum heat treatment of the final cavity can be used to remove excess dislocations. There are many protocols for heat treating niobium, each specific to the desired result, although these have been developed heuristically. Some of the desired results and processes include degassing, annealing, and post purification.

2.2.1 Degassing

Hydrogen atoms, due to their smaller size, can diffuse into the niobium lattice and lodge themselves into interstitial spaces. Hydrogen is an impurity which degrades the bulk properties of niobium. A more serious problem with interstitial hydrogen is the possibility of precipitation of hydrogen atoms on the cavity surface, leading to the formation of hydrides during cooling to operating temperatures [1]. These hydrides degrade the RF performance of the cavity. The hydrogen can be degassed from the niobium by heat treating the niobium at low to medium temperatures. Medium temperature heat treatments, 600 to 800 °C, are performed on cavities at a pressure of $p < 10^{-6}$ Torr. Another method of degassing hydrogen is to bake the cavity at lower temperatures, 100 to 140 °C, for 48 hours [2].

2.2.2 Annealing

Strain and dislocations in the niobium impairs the performance of the cavity by degrading its thermal properties. Heat treating the niobium at medium to high temperatures can reduce the strain in the material by providing energy for sufficient atomic mobility [3]. This process is termed *annealing*. Typical annealing temperatures vary, beginning as low as 800 °C and reaching as high as 2000 °C. Niobium is a refractory metal with a melting point of 2408 °C. Due to the moderate to high temperatures required, a pressure of $p < 10^{-6}$ Torr is crucial to ensure no other impurities are introduced into the niobium. Past research has shown that annealing helps improve the RF performance of the cavity, although it reduces the thermal conductivity and RRR due to diffusion of already present surface impurities into the bulk [4]. To prevent degradation of the thermal conductivity and RRR, an alternate heat treating process was introduced termed *post-purification*, described below.

2.2.3 Post-Purification

As mentioned above, annealing can improve RF performance, but it can reduce the thermal conductivity and RRR. To prevent degradation, a metal with an affinity for the interstitial impurities that is greater than niobium is introduced into the vacuum environment [5, 6]. The greater affinity metal attracts the impurities from the niobium and hence improves the purity of the niobium. These metals are called *getters* and the process is also often called *gettering*. Yttrium has a greater affinity for oxygen than niobium, and hence is a good gettering agent. Titanium is also an effective gettering agent, but it has a lower vapor pressure than yttrium and hence requires higher temperatures or longer heating times. Due to the increased use of titanium for post-purification, the process is also referred to as *titanification*.

Post-purification is carried out at similar temperatures to annealing (1000 to

2000 °C) and in a high vacuum environment ($p < 10^{-6}$ Torr). Titanium and yttrium at temperatures greater than 1200 °C vaporize and adhere to the surface of the niobium. This creates a getter film on the niobium surface, which attracts impurities. The getter film is not good for the RF performance, so the niobium cavity must be subsequently etched in a chemical bath to remove the getter film. Post-purified niobium usually has its RRR increased by a factor of 2 to 3.

2.3 Benefits of heat treating niobium

Heat treatment of niobium, after stamping the sheets into half cells, affects cavity performance and thermal properties like thermal conductivity and Kapitza conductance. The Kapitza conductance is the thermal conductance at grain and surface boundaries. Depending on the type of heat treatment performed, the purity of niobium can also be affected. The following sections outline the benefits of heat treating niobium used for SRF cavities.

2.3.1 Cavity performance

SRF cavities accelerate charged particles through an RF electric field in the interior volume of the cavity. A measure of the efficiency of a cavity is the *quality factor* Q_0, defined as

$$Q_0 = \frac{U}{P_c} \tag{2.2}$$

where U is the energy stored in the cavity and P_c is the energy lost in one radian of the RF cycle. The quality factor indicates the number of oscillations a resonant cavity will go through before dissipating its stored energy [1]. Another measure of performance is the accelerating gradient E_{acc}, which gives the energy imparted to a charged particle per unit length of the cavity. With greater Q_0, the power losses are

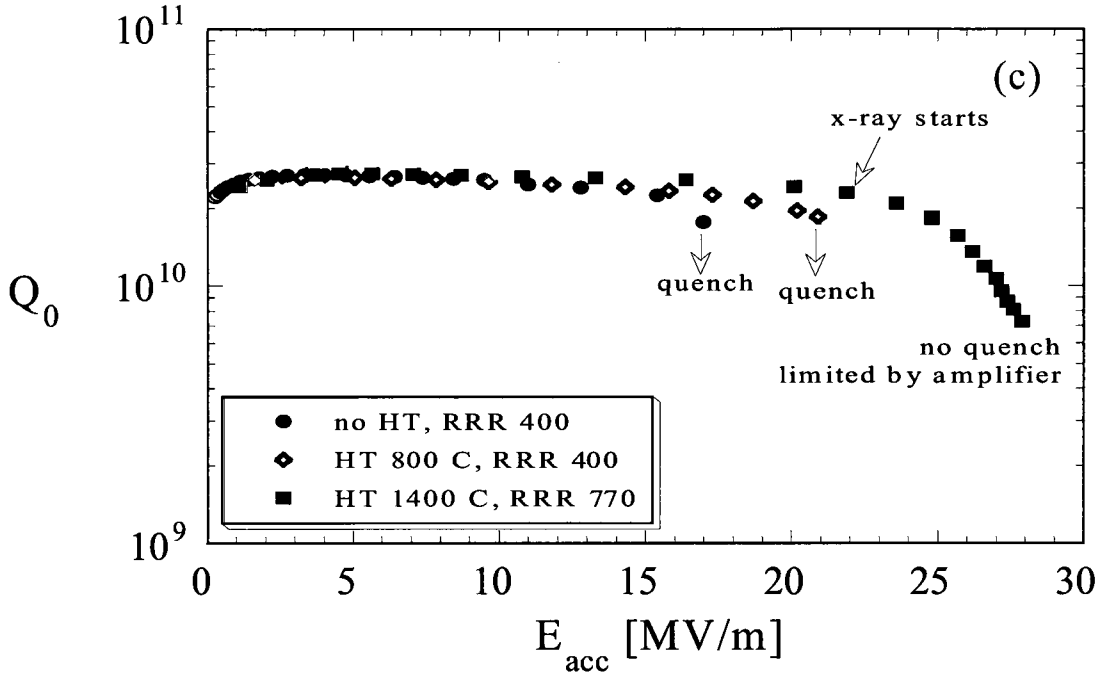

Figure 2.3: Performance of a niobium cavity before and after an 800 °C and a 1400 °C heat treatment [7]. After heat treatment, the cavity produces higher accelerating gradients before quenching, although Q_0 is unchanged. Quenching is due to loss of superconductivity initiated at a local hot spot.

reduced, and with a greater E_{acc}, more energy is imparted to the charged particles.

Heat treating niobium cavities at temperatures above 1200 °C has been shown to improve cavity performance. Figure 2.3 illustrates the improvement of cavity performance after an 800 °C and a 1400 °C heat treatment [7].

The "quench" in Figure 2.3 is due to a location on the cavity heating above the superconducting critical temperature (T_c) of the niobium. Increased thermal conductivity k and Kapitza conductance h_k reduces the possibility of quenching the cavity due to better heat transfer between the interior of the cavity and the helium bath on the outside of the cavity.

The quality factor is also improved at higher accelerating gradients by in situ baking of the niobium cavities at temperatures between 100 – 150 °C for about 48

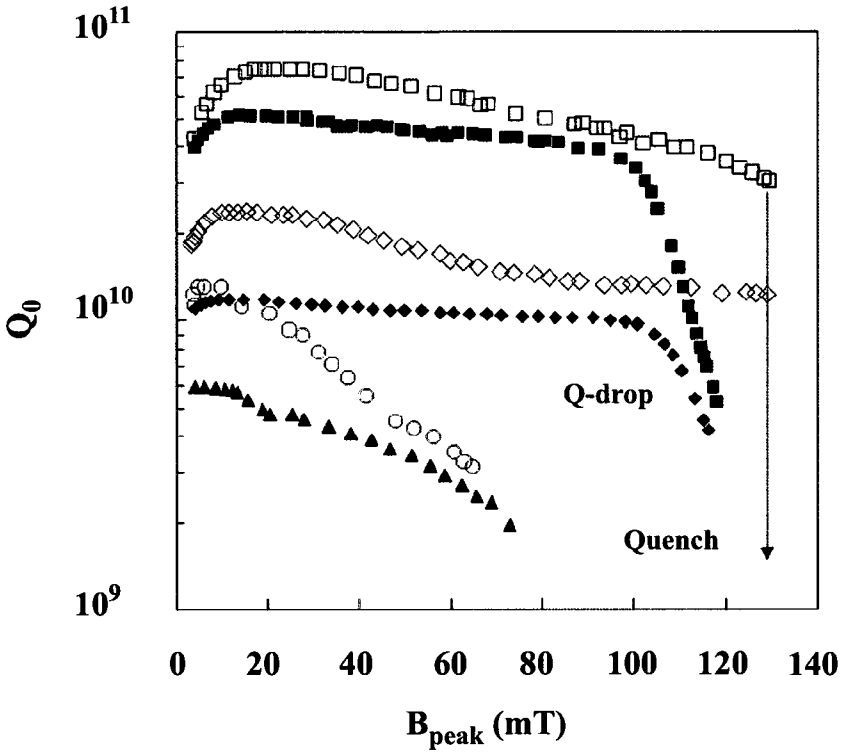

Figure 2.4: Quality factor as a function of magnetic flux before (solid symbols) and after 120 °C 48 h baking (open symbols) at three different temperatures: 1.37 K (squares), 2 K (diamonds), and 2.2 K (circles, triangles) [2].

hours [2, 8]. A comparison of the effect of the in situ low temperature bake for different operating temperatures is illustrated in Figure 2.4 [2].

2.3.2 Thermal properties and purity

Thermal properties, including thermal conductivity and Kapitza conductance (which is analogous to the convection heat transfer coefficient for liquid helium), are important, as they may affect the quench field of a cavity. Heat generated by the RF field on the interior surface of the cavity, sometimes due to surface imperfections, must be dissipated into the surrounding liquid helium bath without affecting superconductivity. Increased thermal conductivity and Kapitza conductance improve the heat

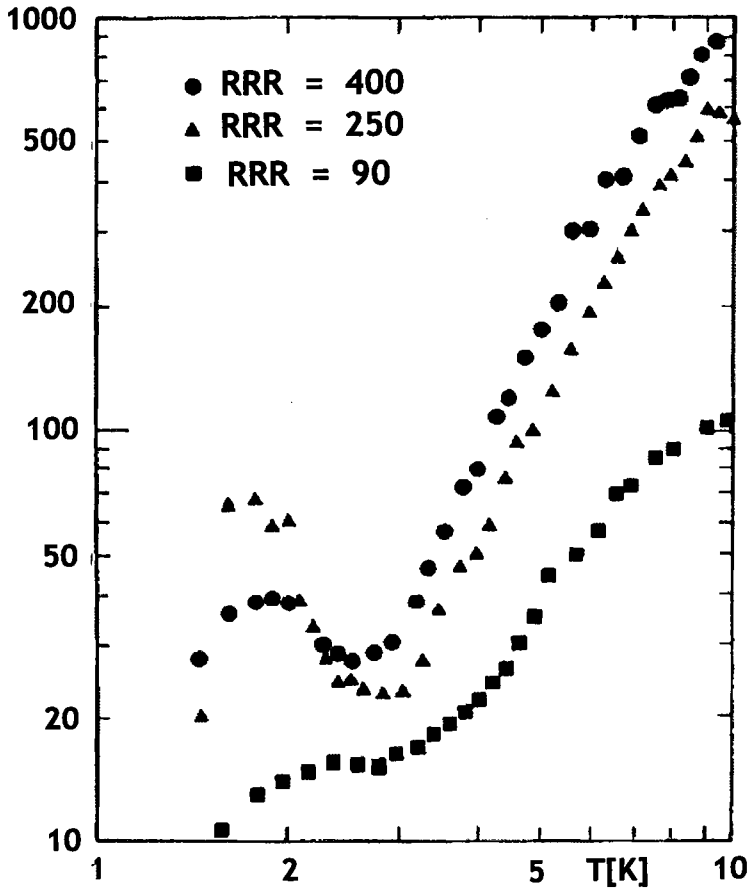

Figure 2.5: Change in thermal conductivity of medium high purity niobium RRR=90 by yttrium treatment (4h 1250 °C → RRR = 400) and HTA (6h 1400 °C → RRR = 250) [9].

transfer from the interior surface of the cavity to the liquid helium.

Heat conduction is comprised of phonon conduction and electron conduction. The contribution due to electron conduction decreases as the temperature decreases. Heat treating niobium at temperatures ranging between 1200 – 2000 °C has proven to increase the thermal conductivity, especially in the phonon conduction region around 2 K [4]. In the absence of a getter material, the purity of niobium decreases, depending on the residual gas pressure within the vacuum furnace.

Improved thermal conductivity can be obtained by improving the purity of the

bulk niobium. Solid state gettering using yttrium [5] or titanium [6] at elevated temperatures has been shown to improve the purity of niobium, hence improving the thermal conductivity and Kapitza conductance. Figure 2.5 illustrates the improvement of RRR and thermal conductivity after a heat treatment of 1250 °C for 4 hours at 10^{-5} Torr (RRR increases from 90 to 400) in the presence of yttrium, and reduced purity after a high temperature annealing (HTA) at 1400 °C for 6 hours in the absence of the getter (RRR decreases from 400 to 250) [9]. Figure 2.6 compares the Kapitza conductance before and after medium temperature (750 °C) heat treatment, titanification of niobium samples, and with the theoretical relation of Bousson [10]. Heat treating niobium increases the Kapitza conductance significantly.

Despite yttrium being a good getter material, it has a higher vapor pressure than titanium and hence more material is vaporized and deposited on niobium. Due to greater costs to acquire yttrium in comparison to titanium, titanium is more widely

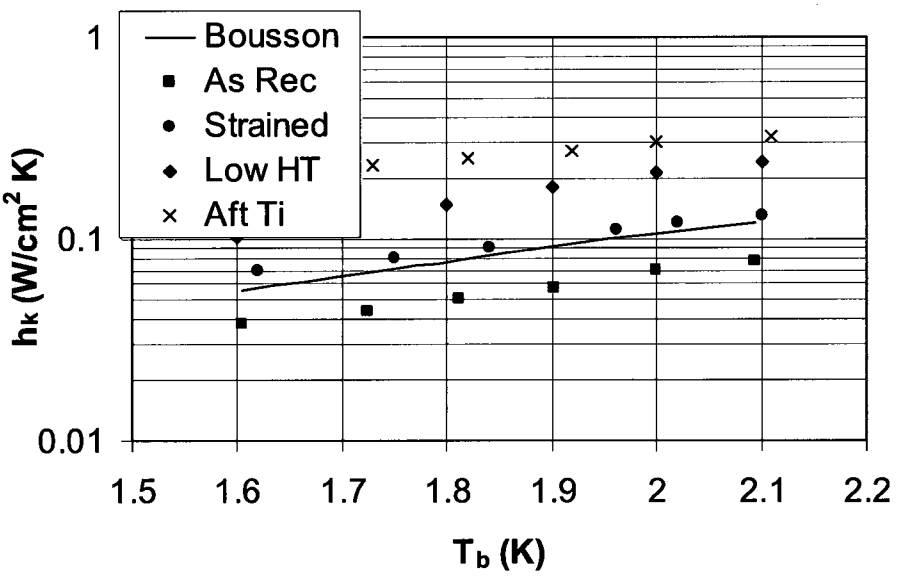

Figure 2.6: Change of the Kapitza conductance of niobium in the "as received" state (squares), after surface indentations to increase surface area (circles), after heat treatment for 2h at 750 °C (diamonds), and after heat treatment for 2h at 1300 °C and 4h at 1200 °C with Ti (crosses). The Bousson correlation is shown [10].

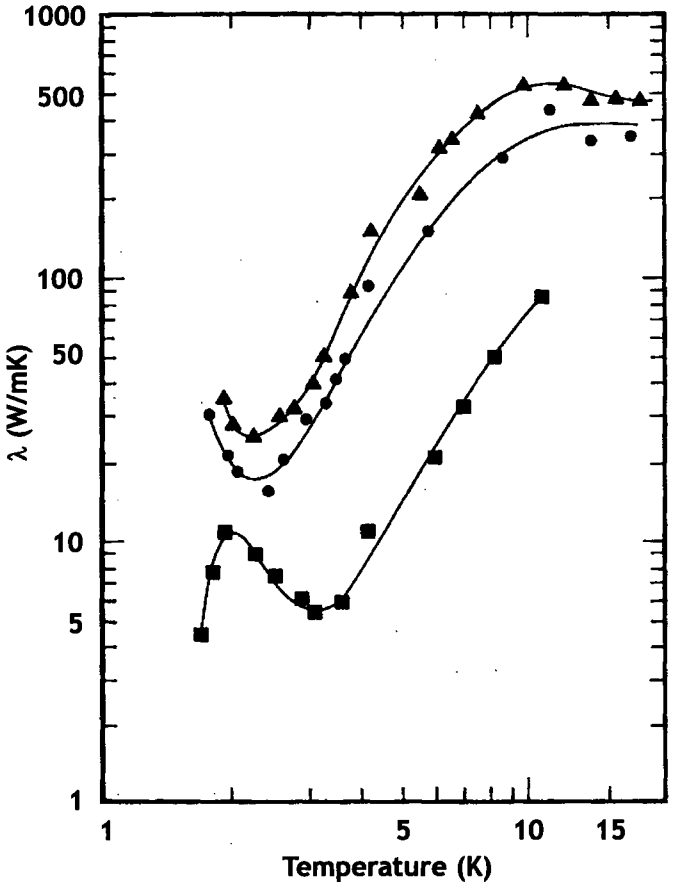

Figure 2.7: Thermal conductivity of a niobium sample after various heat treatments. ■: 2h 2000 °C, •: 6h 1250 °C with Ti gettering, ▲: 10h 1300 °C with Ti gettering [6].

used for solid state gettering. Application of titanium on niobium during the heat treatment produces similar results to that of yttrium, though longer heat treating times are required to compensate for the lower vapor pressure. Figure 2.7 illustrates the effect of various heat treatments with and without titanium, heat treatments being sequentially applied to the niobium sample. The dependence of RRR on heat treating temperature and time [6] on niobium samples with different initial RRR and of various thicknesses is illustrated in Figure 2.8. Studies of the heat treatment with titanium were performed by Safa *et al.* [11, 12] in which the dependence of RRR on the time and temperature of heat treatment was determined, and a semi-empirical model

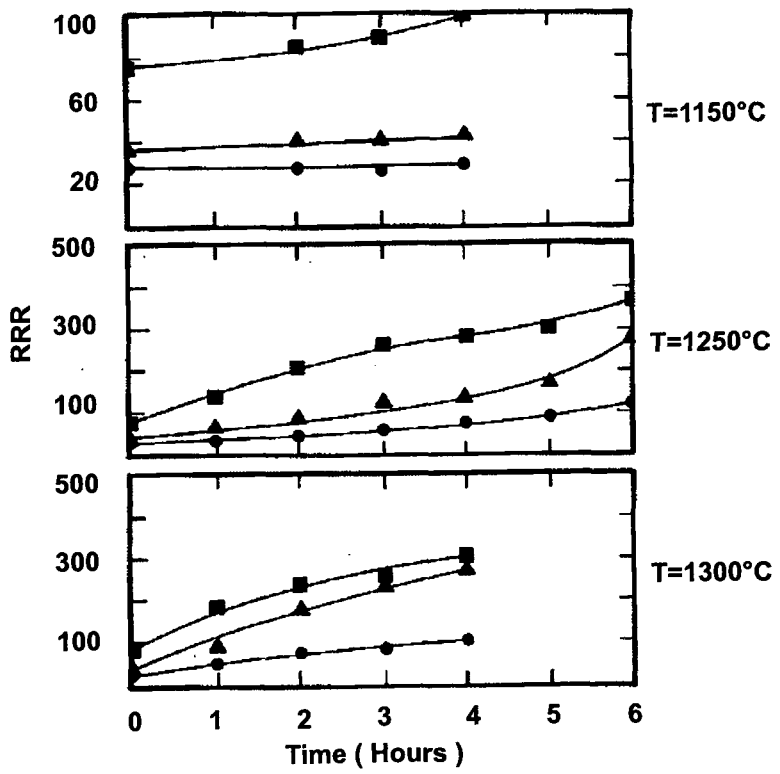

Figure 2.8: Dependence of RRR on the heat treating time and temperature for niobium samples exposed to Ti vapor. •: 1/8″ thick RRR=27, ▲: 1/8″ thick RRR=37, ■: 1/16″thick RRR=77 [6].

to predict RRR was proposed, with reasonable agreement to measured values of RRR after sequential heat treatments. Figure 2.9 illustrates the calculated variation of RRR as a function of the temperature of heat treatment and time. The decrease in RRR or purity of the material after various times is attributed to the contamination of the niobium due to excessive diffusion of titanium into the bulk niobium. The decrease in RRR during heat treatment without titanium, and its increase with titanium is also shown through experiments in [13].

Ongoing research at NSCL and Michigan State University includes the investigation of thermal conductivity, Kapitza conductance, metallurgy, and materials science. Research includes determination of thermal conductivity as a function of the

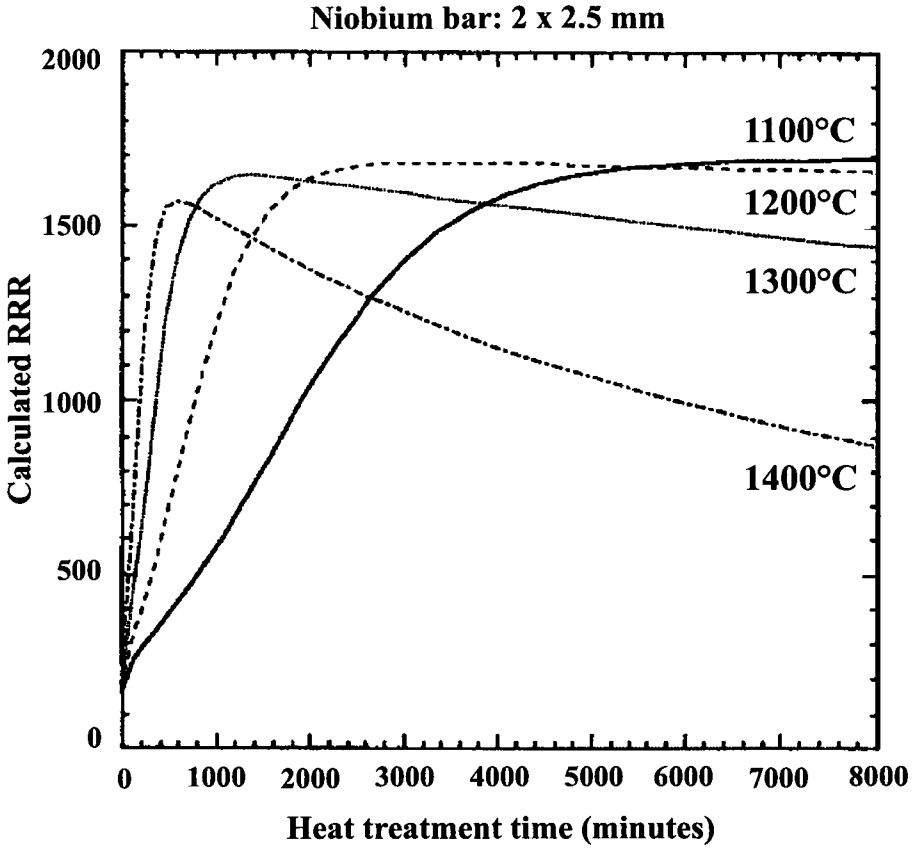

Figure 2.9: Calculated values of RRR as a function of heat treatment temperature and time [11].

processing history, and hence the metallurgy, of niobium [14]; quantifying thermal conductivity and Kapitza conductance as a function of the dislocation density [15]; and determining the relation between thermal conductivity, especially the phonon conduction, and grain orientation of niobium crystals [16]. Materials science research includes the investigation of recovery, recrystallization, and grain growth of niobium after welding and heat treatments [15].

The thermal conductivity of superconducting niobium at temperatures above 3 K is determined by the number of normal electrons available to conduct heat and the purity of the metal. Below 3 K the thermal conductivity is determined by phonon

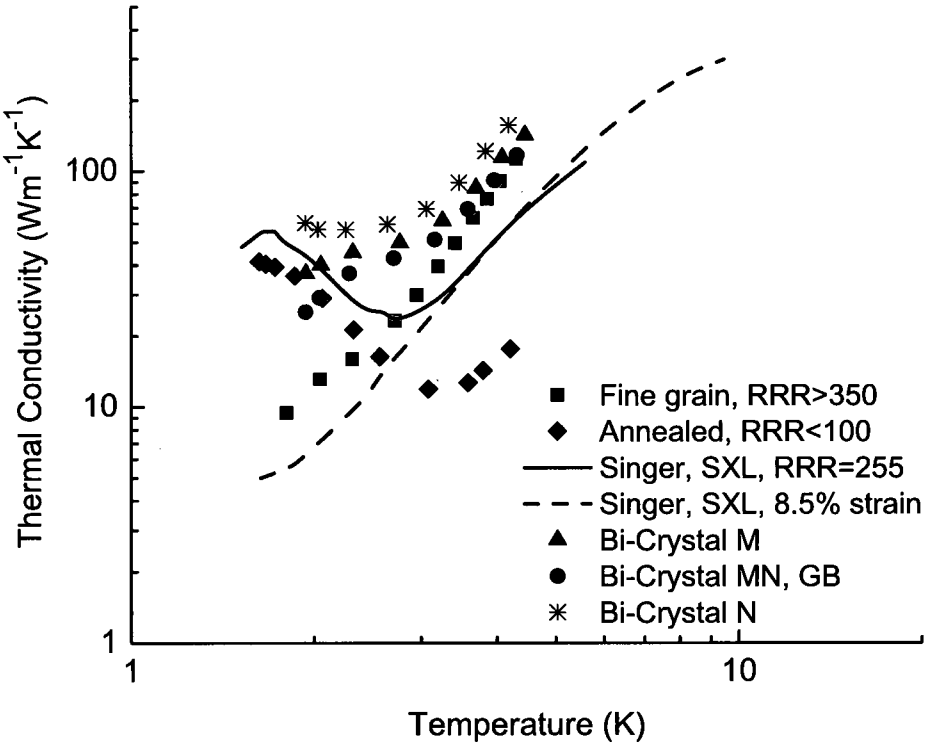

Figure 2.10: Thermal conductivity of several metallurgical states of Nb at low temperature. The single crystal specimen [18] loses its phonon peak after 8.5% tensile strain (dashed line). Our measurements of the small grain specimen reveals that it gains a phonon peak after annealing, but increased impurities (RRR = 350 → 100) reduce k at warmer temperatures. Each of the grains in the bicrystal has greater thermal conductivity than across the grain boundary (GB).

movement, which is dependent on the stress and dislocations in the material. The thermal conductivity at 2 K can be several times that at 3 K due to the presence of a phonon peak. Niobium with 3% [17] and 8.5% [18] strain has shown reduced phonon conduction due to phonon scattering. Figure 2.10 compares the variation of thermal conductivity with temperature for several metallurgical states of niobium.

2.4 Heat Treating Furnace

Despite many studies examining changes in thermophysical properties with metallurgical processing of niobium, many questions remain unanswered. Currently, our laboratory must send specimens to other laboratories for the critical heat treatments. This results in undesired delays in testing protocols. A local furnace to heat treat niobium samples associated with this research will reduce delays for heat treatment of the samples, and provide the researchers with the opportunity to define their own heat treating parameters and determine the effects of such heat treatments. By subjecting a niobium sample (from the actual material being used to fabricate cavities) through a similar path as the fabrication of a cavity, thermal, mechanical, and metallurgical properties can be predicted. With heat treatment being an important step in the fabrication of cavities for high accelerating gradients, a heat treating furnace with the desired temperature and vacuum ranges is essential to the program. Hence, a heat treating furnace has been built to heat treat niobium samples.

Heat treating high purity niobium requires furnaces that can evacuate the heating chamber quickly and maintain a high vacuum through out the process. Another important requirement is to prevent impurity introduction into the niobium from surrounding materials in the furnace. Commercially manufactured heat treating furnaces would require substantial modification to satisfy these requirements, and often are very expensive. Hence, a low-cost, purpose-built research furnace was designed and fabricated to specifically meet the requirements of NSCL. First, a prototype furnace was constructed and tested, and the test results were compared with design calculations. With the prototype results and analytical predictions, the specific requirements of the research furnace were evaluated and the furnace was designed.

Chapter 3

Design Calculations and Prototype Furnace

A prototype furnace was built to provide insight into the choice of material, design and fabrication techniques, and workability of the materials used. This furnace was fabricated from material and equipment already available at NSCL. The aim in the prototype was to melt a copper cylinder of diameter 0.051 m ($2''$) and length 0.076 m ($3''$) and account for the electrical power input into the furnace.

A salvaged cylindrical steel vessel of length 0.610 m ($24''$) and inner diameter of 0.230 m ($8''$) with five conflat flanges already welded on it was chosen for the vacuum vessel of the prototype furnace. A CAD drawing of the part is shown in Figure 3.1. All of the other components were designed and acquired based on the dimensions of this vessel.

The other important components of the furnace were divided into the electrical system, thermal shields, vacuum system, and thermometry.

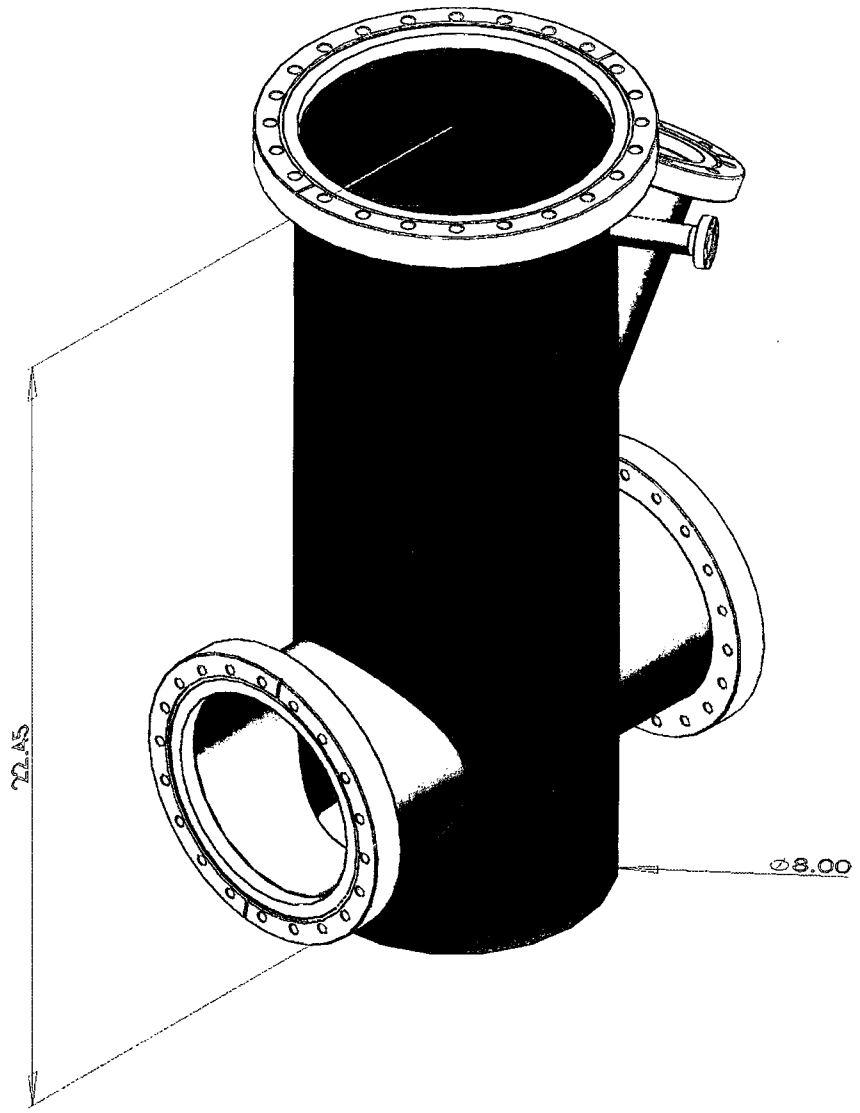

Figure 3.1: Steel vessel with pre-welded conflat flanges used for the furnace's vacuum vessel.

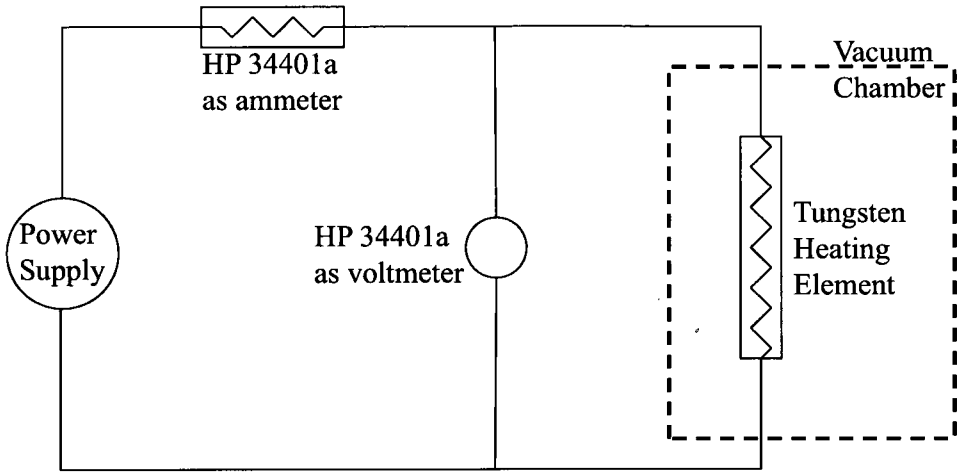

Figure 3.2: Circuit diagram of the electrical system for the prototype furnace.

3.1 Electrical system

The electrical system is composed of a variable transformer power supply, insulated electrical leads on the atmospheric side, a vacuum electrical feed-through to transmit electricity from the atmospheric side to the vacuum side of the furnace, and the electrical heating element in the vacuum side. A standard variable transformer was used as the power supply for the prototype furnace, and was connected to the vacuum feed-through with 12 gauge insulated copper wires. An ammeter was connected in series with the insulated copper wires, and a voltmeter was connected in parallel with the circuit. Two Hewlett-Packard 34401a high performance bench-top multimeters were used as the voltmeter and ammeter. A hand held multimeter was also used periodically to double-check the readings of the bench-top multimeters. A schematic drawing of the electrical system for the prototype furnace is illustrated in Figure 3.2.

Table 3.1: Comparison of refractory metals with little influence on niobium purity. Properties not available indicated with an "N/A".

Refractory Metal	**Cost ($/m, ø0.02″) [19]**	**Melting temperature (°C) [20]**	**Thermal conductivity at 1800 K ($W\,cm^{-1}K^{-1}$) [20]**	**Thermal expansion coefficient at 800 K (K^{-1}) [20]**
Molybdenum	5.06	2617	0.907	5.7×10^{-6}
Niobium	84.10	2408	0.764	N/A
Rhenium	471.00	3180	N/A	N/A
Tantalum	23.90	2996	0.634	7.1×10^{-6}
Tungsten	9.22	3410	1.03	4.8×10^{-6}

A two lead electrical feed-through was acquired from MDC vacuum. The feed-through had a 0.069 m (2.73″) diameter conflat flange for a vacuum seal using a copper gasket. The electrical leads were made of copper and were insulated from the flange by a ceramic standoff.

3.1.1 Selection of Heating Element

The desire not to introduce impurities, along with the design temperature of about 1500 °C, provided an opportunity to test the suitability of a few candidate metals for the heating element. These requirements narrow the choices for the heating element, as few metals are known to have a small diffusion coefficient into niobium. At the same time, few metals are capable of withstanding the high temperature of operation. The later metals are referred to as refractory metals and include molybdenum, niobium, rhenium, tantalum and tungsten. Table 3.1 lists the criteria used for making a selection for the heating element from the group of refractory metals. From Table 3.1, some of the choices can be eliminated due to their high cost. To select among the remaining choices, diffusion of these metals into niobium was quantified and compared with the amount of diffusion of yttrium and titanium.

Niobium is heat treated to improve its purity and thermal conductivity, for example. At elevated temperatures, with the presence of other metals and gases, it is possible to contaminate niobium. Hence, diffusion into niobium of the various metals present in the furnace in the form of shields and heating elements must be examined, and compared to the diffusion of yttrium and titanium into niobium. Despite yttrium being a good getter metal, titanium is typically used as the getter due to its lower cost. This comparison to titanium is performed since titanium is introduced into the heating chamber during the titanification process, and then a suitable thickness of the resulting oxide is etched off in an acid bath after the heat treatment. Hence, any of the metals with a lower diffusion than titanium would be acceptable. But, since there are heating processes when titanium will not be introduced, it is important to choose a metal that diffuses the least into the niobium. The distance diffused x into the niobium can be estimated as

$$x = \sqrt{Dt} \tag{3.1}$$

where D is the diffusion coefficient and t is time of diffusion. The diffusion coefficient can be calculated, using an Arrhenius equation, as

$$D = A \exp\left(\frac{-E_a}{RT}\right) \tag{3.2}$$

where A is the frequency factor, E_a is the activation energy, R $\left(= 1.987 \text{ cal.mol}^{-1}\text{K}^{-1}\right)$, and T is the temperature. Values for A and E_a [21] for molybdenum, tantalum, titanium, tungsten and yttrium diffusing into niobium are listed in Table 3.2. The estimated values of the diffusion distance of the select refractory metals into niobium at 1500 °C and 1250 °C is illustrated in Figure 3.3. Figure 3.3 indicates that tungsten diffuses by the smallest amount, making it the best choice for the heating element and other parts of the furnace.

Table 3.2: Values of the frequency factor A, activation energy E_a, and diffusion coefficients at 1250 °C and 1500 °C for diffusion of select refractory metals into niobium. Table adapted from [21].

Metal	Frequency factor A (cm^2/s)	Activation energy E_a (kcal/mol)	Diffusion coefficient D (cm^2/s)	
			1250 °C	1500 °C
Molybdenum	92	122	2.85×10^{-16}	8.40×10^{-14}
Tantalum	1	99.3	5.61×10^{-15}	5.74×10^{-13}
Titanium	0.4	88.5	7.97×10^{-14}	4.92×10^{-12}
Tungsten	70000	156	2.87×10^{-18}	4.11×10^{-15}
Yttrium	0.0015	55.6	1.57×10^{-11}	2.10×10^{-10}

3.1.2 Electrical resistance of tungsten

Any electrical conductor offers a resistance to the flow of electrons. How strongly a conductor offers resistance to the flow of current is termed as the electrical resistivity ρ. The electrical resistance R of the conductor and resistivity ρ can be related in one dimension as

$$\rho = R\frac{A}{l} \tag{3.3}$$

where A is the cross sectional area of the conductor normal to the EMF, and l is the length of the conductor.

Values of the temperature dependent electrical resistivity and thermal expansion for tungsten are published in [22], and are listed in Table 3.3. The resistance of the tungsten heating element in the furnace can be estimated by taking into account the thermal expansion of the tungsten which affects the length of the wire, and the resistivity values listed in Table 3.3.

3.1.3 Forming the heating element

Despite the advantage of lower diffusion rate into niobium, tungsten has a few drawbacks as the heating element. In general, tungsten is difficult to work with at room

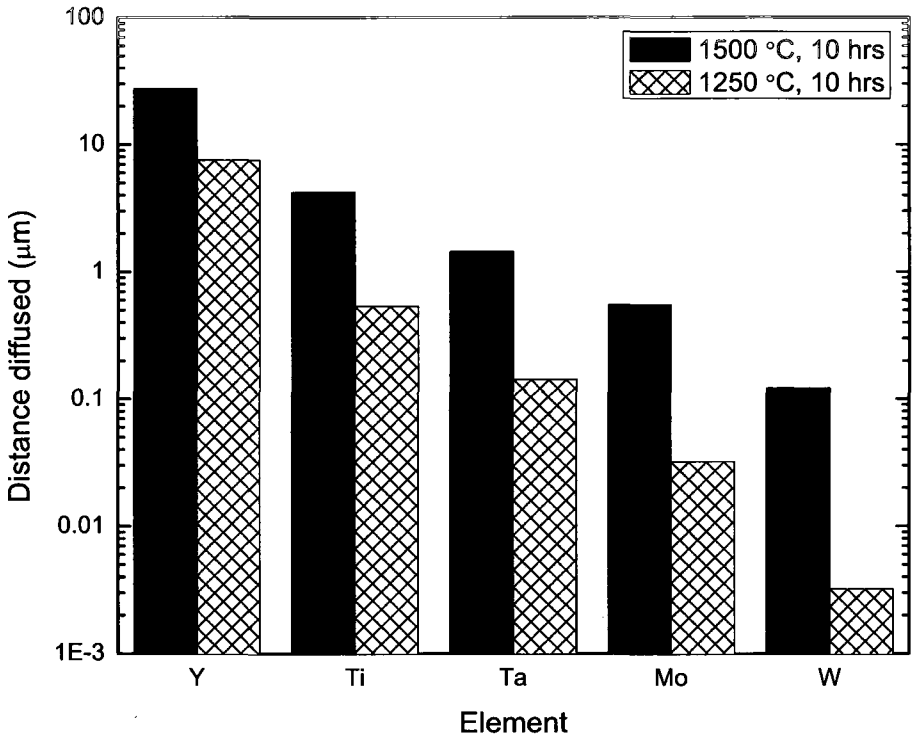

Figure 3.3: Estimated diffusion of select refractory metals into niobium at 1500 °C and 1250 °C, in comparison yttrium and titanium.

temperature due to its brittle nature and hence requires heating of the section being formed and special tools. An exception exists for the simple forming of fine wire of diameters less than or equal to 7.62×10^{-4} m (0.030″) [23]. Hence tungsten wires of diameters 5.08×10^{-4} m (0.020″) and 7.62×10^{-4} m (0.030″) were acquired from Alfa Aesar® and were formed into heating elements to check formability and workability with standard tools.

The length of wire needed for the coil was determined using Equation (3.3) and the Joule heating relation

$$P = VI = I^2R \tag{3.4}$$

Table 3.3: Values of the temperature dependent electrical resistivity ρ and thermal expansion of tungsten. Table adapted from [22].

Temperature (K)	**Electrical resistivity ρ ($\mu\Omega$cm)**	**Thermal expansion (%) l_o at 293 K**
300	5.65	0.003
400	8.06	0.044
500	10.56	0.086
600	13.23	0.130
700	16.09	0.175
800	19.00	0.222
900	21.94	0.270
1000	24.93	0.320
1100	27.94	0.371
1200	30.98	0.424
1300	34.08	0.479
1400	37.19	0.535
1500	40.36	0.593
1600	43.55	0.652
1700	46.78	0.713
1800	50.05	0.775
1900	53.35	0.839
2000	56.67	0.904
2100	60.06	0.971
2200	63.48	1.039
2300	66.91	1.109
2400	70.39	1.180
2500	73.91	1.253
2600	77.49	1.328
2700	81.04	1.404
2800	84.70	1.479
2900	88.33	1.561
3000	92.04	1.642
3100	95.76	1.724
3200	99.54	1.808
3300	103.3	1.893
3400	107.2	1.980
3500	111.1	2.068
3600	115.0	2.158
3655	117.1	2.209

where P is the power dissipated, V is the voltage applied, I is the current flowing through the conductor, and R is the resistance of the electrical conductor. Substituting for R from Equation (3.3) into Equation (3.4),

$$P = I^2 \rho \frac{l}{A} \tag{3.5}$$

To determine the length of the coil, the power required P was estimated, as explained in Section 3.2. The current I was approximated using a tungsten filament properties nomogram (Figure 3.4) [23], estimating a requirement of 11 amperes for a tungsten wire of diameter 7.62×10^{-4} m at a temperature of 1127 °C. A current requirement of 15 amperes was assumed to account for the wound coil instead of a straight wire, and for a power requirement of 200 W, the length of wire for the coil was estimated to be 1.09 m.

Tungsten when cold wound into a coil has a spring effect and hence, requires a mandrel with a smaller diameter than the desired element coil diameter. For the prototype furnace, the heating element was to have a diameter of 25.4×10^{-3} m. A special mandrel, shown in Figure 3.5, was fabricated from a threaded stainless steel rod with a diameter of 19.05×10^{-3} m. The threaded stainless steel rod was drilled to make it hollow to accommodate the tungsten lead returning to the feed-through from the bottom end of the element. Tungsten wire of diameter 7.62×10^{-4} m, when wound on this custom mandrel, had a final diameter of 21.6×10^{-3} m which was acceptably close to the 25.4×10^{-3} m diameter target. Care was taken while forming the bends of angle $\geq 90°$ in the coil, and radii of the bends were greater than twice the diameter of the wire (i.e., radius $\geq 15.2 \times 10^{-4}$ m) to prevent the wire from cracking [23].

The final coil that was wound on the mandrel and used in the prototype furnace as the heating element is pictured in Figure 3.6.

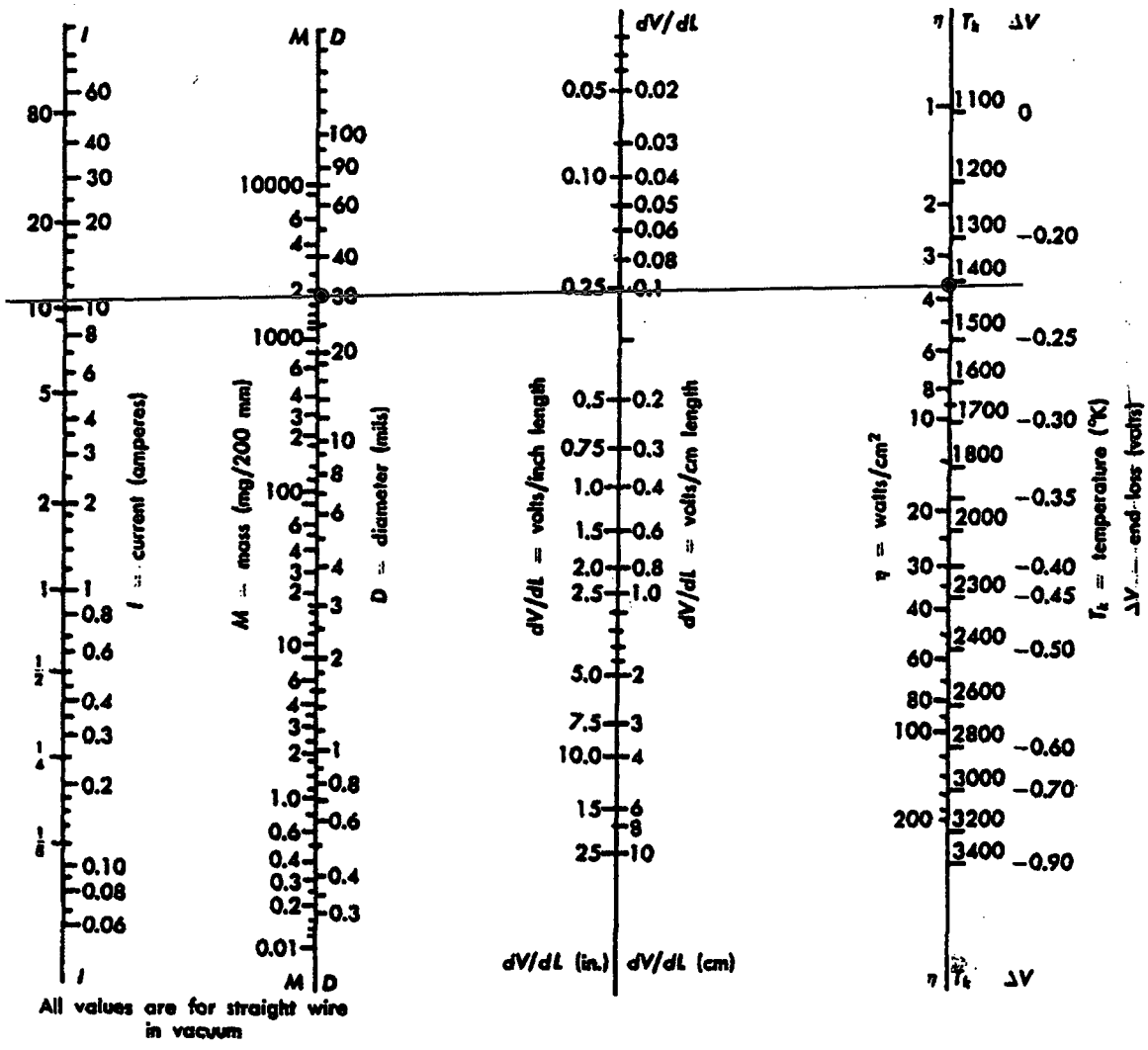

Figure 3.4: Nomogram relating the properties of tungsten straight wire in vacuum [23]. The line drawn across the nomogram is for a wire of diameter 7.62×10^{-4} m (30 mils) and temperature of 1127 °C (1400 K), estimating a requirement of 11 amperes of current and a voltage of 0.1 volts/cm length of wire.

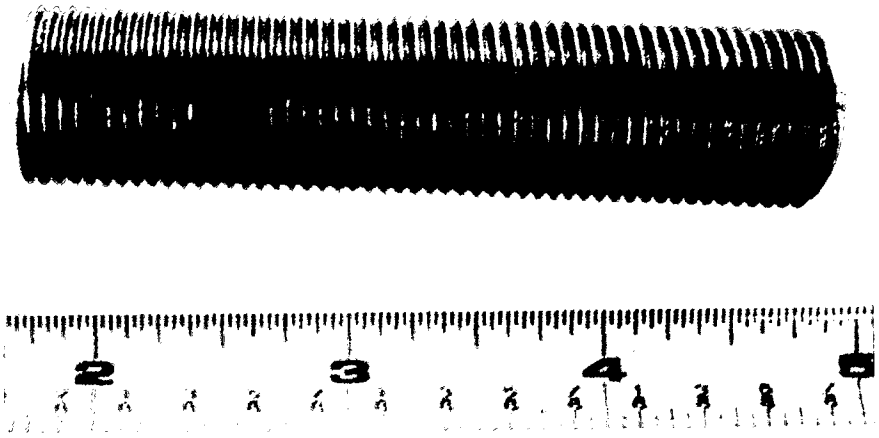

Figure 3.5: Custom fabricated stainless steel mandrel for winding tungsten wire into a coil of diameter 25.4×10^{-3} m ($1''$).

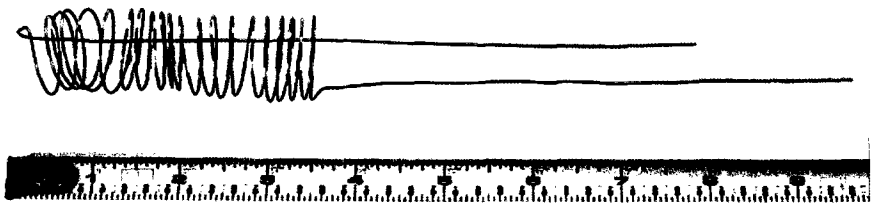

Figure 3.6: Heating element fabricated from tungsten wire using the mandrel shown in Figure 3.5. The wire used to fabricate the heating element pictured above was of diameter 7.62×10^{-4} m ($0.03''$).

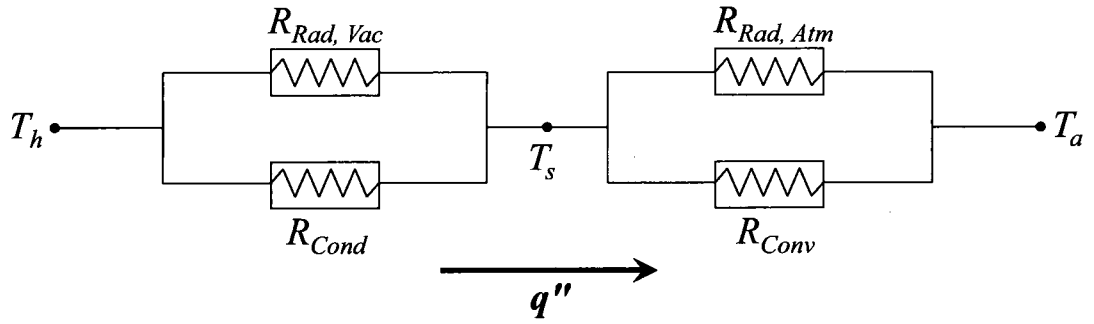

Figure 3.7: Resistance network model for heat losses in a vacuum furnace, where T_h is the temperature at the hot zone of the furnace, T_s is the temperature at the outer surface of the furnace wall, and T_a is the ambient temperature. $R_{Rad,Vac}$ is the resistance due to radiation within the furnace in vacuum, $R_{Rad,Atm}$ is the resistance due to radiation from the outer surface of the furnace wall to the surrounding atmosphere, R_{Cond} is the resistance due to conduction through structural parts, and R_{Conv} is the resistance due to convection from the outer surface of the furnace wall to the surrounding atmosphere.

3.2 Thermal shields

In a vacuum furnace, the heat loss consists mainly of radiation heat transfer, small amounts of conduction due to structural parts, and convection and radiation from the outer surface of the furnace to the surroundings. The thermal design is based on the steady state response. A resistance network of the heat loss in a vacuum furnace, consisting of radiation from the hot zone of the furnace to the cooler outer wall of the furnace, conduction from the hot zone through various support structures, radiation from the outer wall of the furnace to the surrounding atmosphere and convection from the outer wall to the atmosphere, is shown in Figure 3.7.

The total heat loss q_{total} from the vacuum furnace can also be written as

$$q_{total} = q_{rad} + q_{cond} + q_{conv} \tag{3.6}$$

where q_{rad} is the heat loss due to radiation, q_{cond} is the heat loss due to conduction,

and q_{conv} is the heat loss due to convection. At the high operating temperature of the furnace, the heat transfer from the outer surface of the furnace to the surrounding atmosphere is dominated by radiation due to the high temperature difference and due to convection being natural convection only. Hence only radiation from the outer surface is taken into account in the calculations performed for the prototype furnace.

3.2.1 Radiation heat transfer

The radiation heat loss from the hot zone of the furnace to the surrounding atmosphere through the outer wall of the furnace can be estimated using Stefan-Boltzmann law and assuming gray body behavior as

$$q_{rad} = \frac{\sigma \left(T_h^4 - T_c^4\right)}{R} \tag{3.7}$$

where σ is the Stefan-Boltzmann constant ($\sigma = 5.669 \times 10^{-8}$ W.m^{-2}K^{-4}), T_h is the absolute temperature of the hot zone, T_c is the absolute temperature of the surrounding atmosphere, and R is the resistance to radiation heat transfer. The resistance R in Equation (3.7) accounts for the presence of radiation shields and takes into account view factors of the surfaces between which radiation heat transfer occurs. A schematic representation of the radiation heat transfer in the prototype furnace and a resistance network for determining the resistance R is illustrated in Figure 3.8.

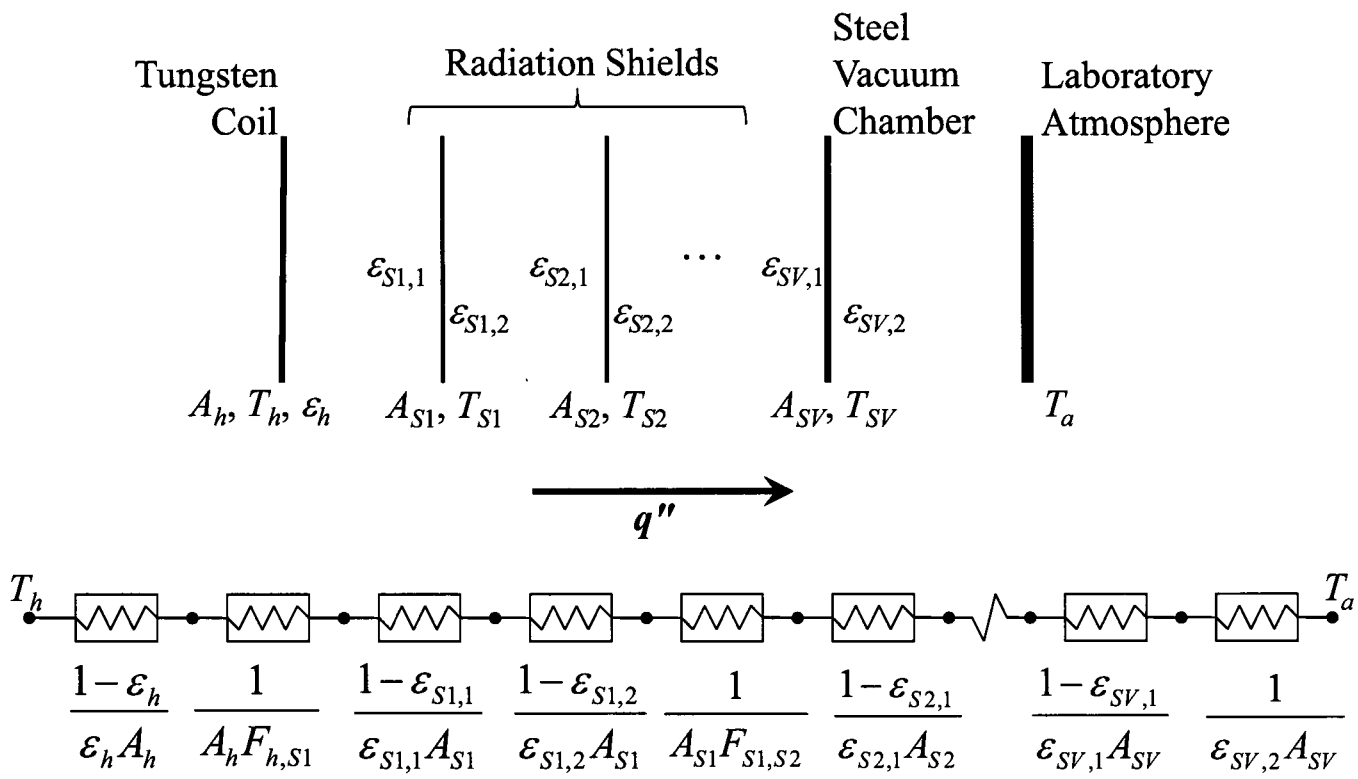

Figure 3.8: Schematic representation of the radiation heat loss in the prototype furnace, with losses from the tungsten to the atmosphere surrounding the furnace. A resistance network to determine R in Equation (3.7) is also shown. The subscript h refers to the hot tungsten, a the cooler atmosphere, Si the radiation shield i with $i = 1, 2, \ldots, n$ and n being the total number of shields, SS the stainless steel chamber, and $Si, 1$ and $Si, 2$ the two sides of shield i, respectively. T is the absolute temperature of the various surfaces, A the surface area of the components, ϵ the emissivity, and F the view factor.

The resistance R in Equation (3.7) can be written as

$$R = \frac{1-\epsilon_h}{\epsilon_h A_h} + \frac{1}{A_h F_{h,S1}} + \frac{1-\epsilon_{S1,1}}{\epsilon_{S1,1} A_{S1}} + \frac{1-\epsilon_{S1,2}}{\epsilon_{S1,2} A_{S1}} + \frac{1}{A_{S1} F_{S1,S2}} + \frac{1-\epsilon_{S2,1}}{\epsilon_{S2,1} A_{S2}} + \cdots + \frac{1-\epsilon_{SS,1}}{\epsilon_{SS,1} A_{SS}} + \frac{1}{\epsilon_{SS,2} A_{SS}} \tag{3.8}$$

where the subscript h refers to the hot tungsten, c the cooler atmosphere, Si the radiation shield i with $i = 1, 2, \ldots, n$ and n being the total number of shields, SS the stainless steel chamber, and $Si, 1$ and $Si, 2$ the two sides of shield i, respectively. T is the absolute temperature of the various surfaces, A the surface area of the components, ϵ the emissivity, and F the view factor. The view $F_{h,S1}$ is defined as the fraction of radiation leaving surface h that is intercepted by surface $S1$ [24].

The reduction in radiation losses by adding radiation shields in the prototype vacuum furnace is shown in Figure 3.9. The reduction of radiative losses by the addition of each shield is calculated as $(P_{ns} - P_s) * 100/P_{ns}$, where P_{ns} is the power when no shields are present and P_s is the power when one or more shields are present, and is included on the right ordinate of Figure 3.9. Despite the reduction in losses with each additional shield, there is a diminishing return for each additional shield, amounting to less than 1% per shield for shields 9 and above.

For the prototype, copper sheets were used for the thermal shields due to their availability and ease of formability. Due to the cylindrical shape of the vacuum vessel, the thermal shields were designed as concentric copper cylinders held together by stainless steel screws and nuts. Nine layers of thermal shields were installed, of height 24.8×10^{-2} m and diameters ranging from 12.7×10^{-2} m to 17.8×10^{-2} m, in increments of 6.35×10^{-3} m. Two smaller center shields were also installed to contain the molten copper of the 0.0508 m copper target cylinder. The cylindrical radiation shields installed inside the vacuum vessel are shown in Figure 3.10.

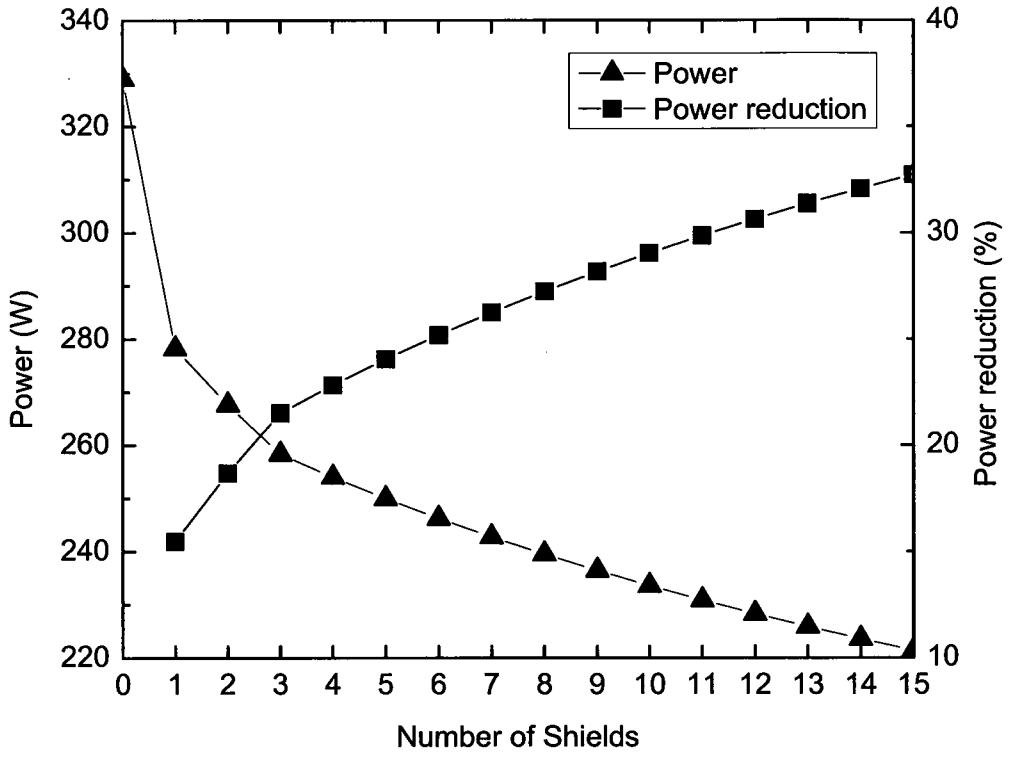

Figure 3.9: Estimated power consumption as a function of the number of radiation shields for the prototype furnace, for a hot-zone temperature of 1200 °C. Reduction of power consumption by the addition of each shield in comparison to the zero shields case is plotted on the right ordinate.

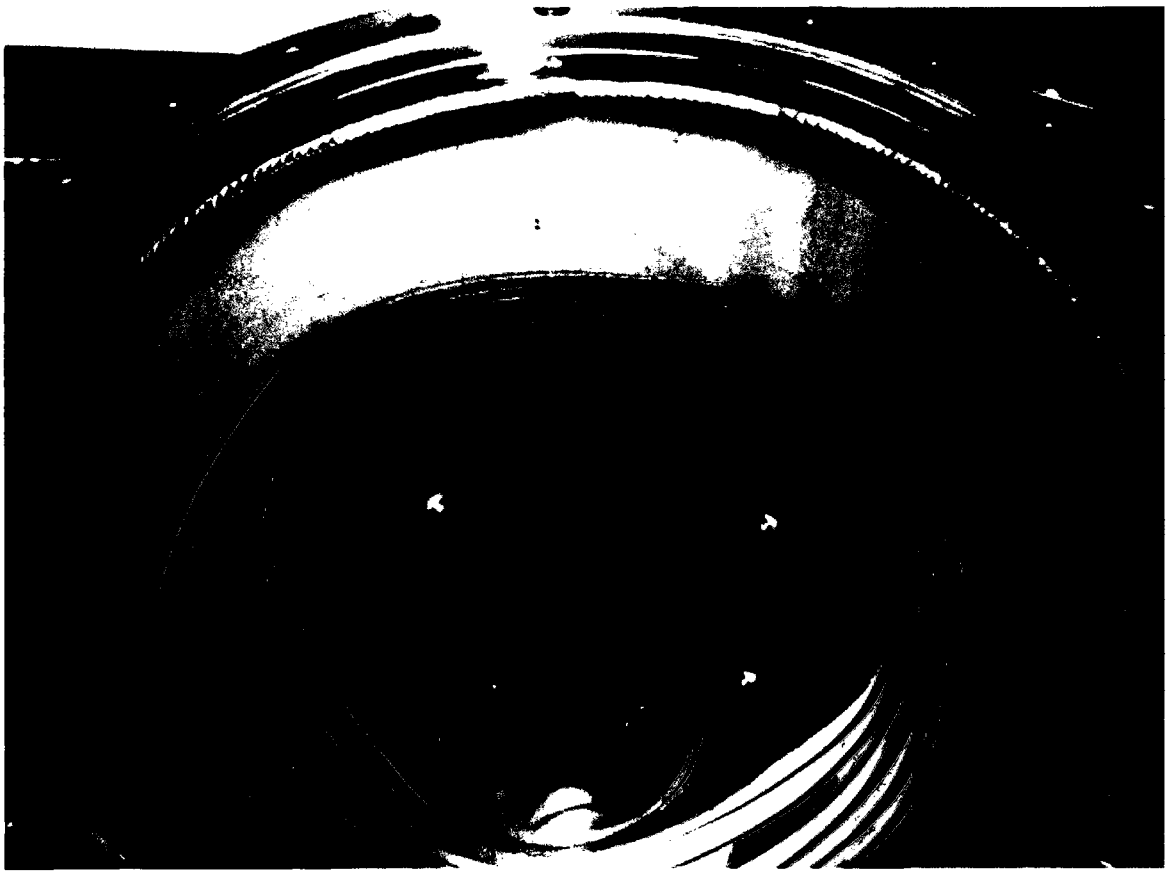

Figure 3.10: Copper thermal radiation shields placed within the vacuum vessel to reduce heat losses due to radiative heat transfer. The concentric circular assumption in modeling is an idealization.

3.2.2 Conduction heat transfer

Despite the need to reduce heat losses, structural components are needed, including screws, nuts, ceramic supports, and feed-throughs. These parts are exposed to the hot zone on one end and pass through the radiation shields to the cooler outer wall of the furnace, conducting heat away from the hot zone. These conduction heat losses are determined using the steady state heat conduction equation with temperature dependent thermal conductivity to account for the temperature gradient across the individual parts, and written as

$$\frac{d}{dx}\left(k\frac{dT}{dx}\right) = 0 \tag{3.9}$$

For structural support and for spacing the shields, twelve stainless steel screws of diameter 0.00251 m and length 0.0381 m were used on the cylindrical shields. Three alumina tubular supports of inner diameter 0.00158 m and outer diameter 0.00476 m and length 0.152 m were used to hang the upper circular shields from the 0.254 m diameter end cover. Due to the large length to diameter ratios of 15 and 32 for the stainless steel screws and alumina tubes, respectively, one dimensional heat conduction was assumed for calculations.

Heat conduction through the stainless steel screw and nut setup, and through the alumina rods were calculated from Equation (3.9), using the temperature dependent thermal conductivity for stainless steel [25],

$$k = 7.9318 + 0.023051 \times T - 6.4166 \times 10^{-6} \times T^2 \tag{3.10}$$

and for alumina [26],

$$k = 5.85 + \frac{15360 \times \exp(-0.002 \times T)}{T + 516} \tag{3.11}$$

The thermal conductivities for stainless steel and alumina as a function of temperature as determined using Equations (3.10) and (3.11), respectively, are illustrated in Figure 3.11. Integrating Equation (3.9),

$$k\frac{\partial T}{\partial x} = C_1 \tag{3.12}$$

and substituting for k in Equation (3.12) with, for example, Equation (3.10), gives

$$\left(7.9318 + 0.023051 \times T - 6.4166 \times 10^{-6} \times T^2\right)\frac{\partial T}{\partial x} = C_1 \tag{3.13}$$

Integrating,

$$7.9318 \times T + 0.011525 \times T^2 - 2.1388 \times 10^{-6} \times T^3 = C_1 \times x + C_2 \tag{3.14}$$

Assuming the temperatures at the two ends of the screws to be equal to the temperatures of the copper radiation shields coincident with the ends, C_1 and C_2 can be determined. Hence, temperatures at any location on the screws could be computed. For one dimensional heat conduction, heat loss due to conduction through the screws was estimated by determining the heat flux through an infinitesimally small cross sectional volume of the screw, as illustrated in Figure 3.12. The length of the infinitesimally small cross sectional volume was assumed to be one hundredth the length of the screw. At the operating temperature of the prototype furnace, a gradient of 3 °C was estimated over the length of the infinitesimally small section of the screw, and the corresponding difference in thermal conductivity at the two ends of the infinitesimally small section was 0.16 %. Hence, the thermal conductivity of the infinitesimally small cross sectional volume of the screw was assumed to be the thermal conductivity estimated at the hotter end for that screw. Therefore, the

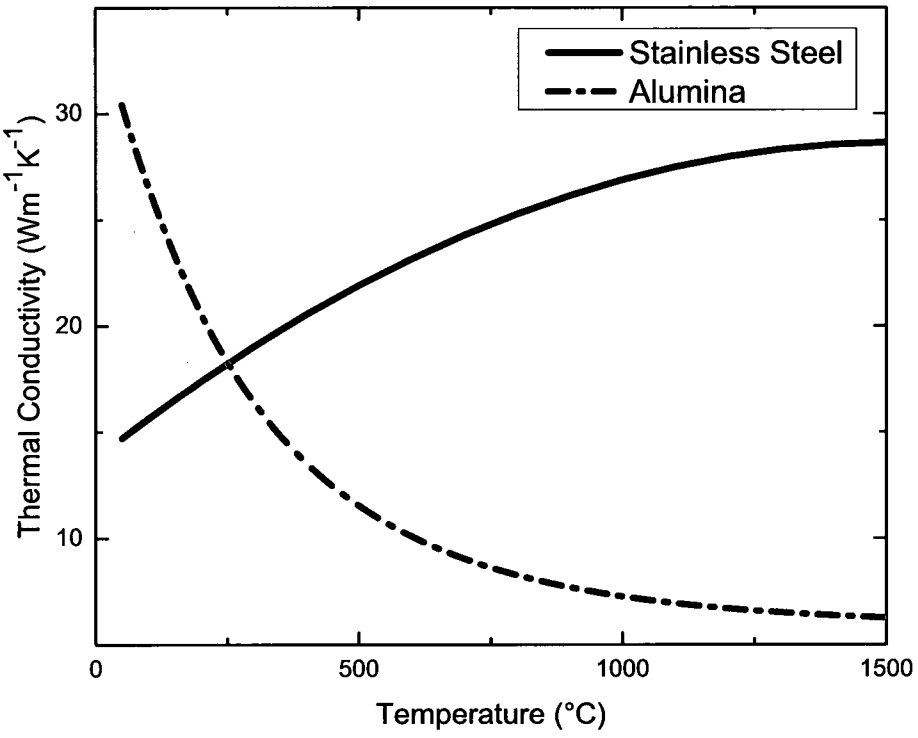

Figure 3.11: Comparison of the thermal conductivities of stainless steel [25] and alumina [26]. The advantage of using alumina for temperatures hotter than 250 °C is clear.

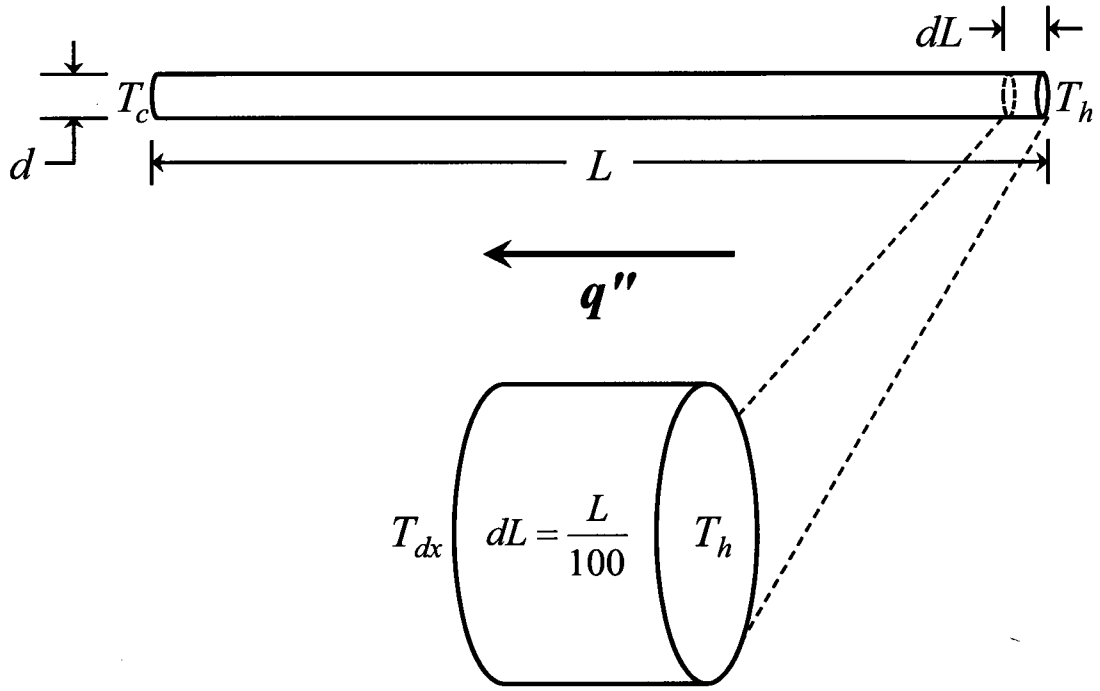

Figure 3.12: Infinitesimally small cross sectional volume assumption to determine heat loss due to conduction through stainless steel screws and alumina tubes. For a furnace coil temperature of 1100 °C, $T_x - T_{dx}$ was approximately 3 °C and difference in thermal conductivity was 0.16 %.

conduction heat loss was estimated as

$$q_{cond} = k_h A \frac{T_h - T_{dL}}{dL} \tag{3.15}$$

where k_h is the thermal conductivity at T_h, A the cross sectional area of the screw, T_h the absolute temperature at the hot end of the infinitesimally small section of the screw, T_{dL} the estimated temperature at length dL from the hot end of the screw, and dL the length of the infinitesimally small section of the screw.

At 1000 °C, heat conduction through the stainless steel screws and nuts contribute about 10 % of the total calculated heat loss, and the alumina rods contribute 2 %. At cooler temperatures, though, the alumina rods account for a greater fraction of heat conduction losses due the exponential decay of the thermal conductivity with increasing temperature. For example, at 200 °C, conduction through stainless steel screws and nuts contribute to 34 % of the total calculated heat loss, and the alumina rods contribute to 30 %.

3.3 Vacuum system

The absence of gaseous impurities like oxygen, nitrogen, and hydrogen from the heating environment ensures reduced impurity introduction into the niobium being heat treated. A high vacuum on the order of 10^{-5} – 10^{-6} Torr provides the required environment for heat treatment. To achieve this vacuum and evacuate the vacuum chamber in a reasonable time, a Varian Vacuum Technologies diffusion pump (model VHS-4) with an operating range of 1×10^{-3} – 5×10^{-9} Torr and a 1200 L/s pumping speed was used in conjunction with a mechanical backing pump (roughing pump). A schematic diagram of the vacuum system used for the prototype furnace is shown in Figure 3.13.

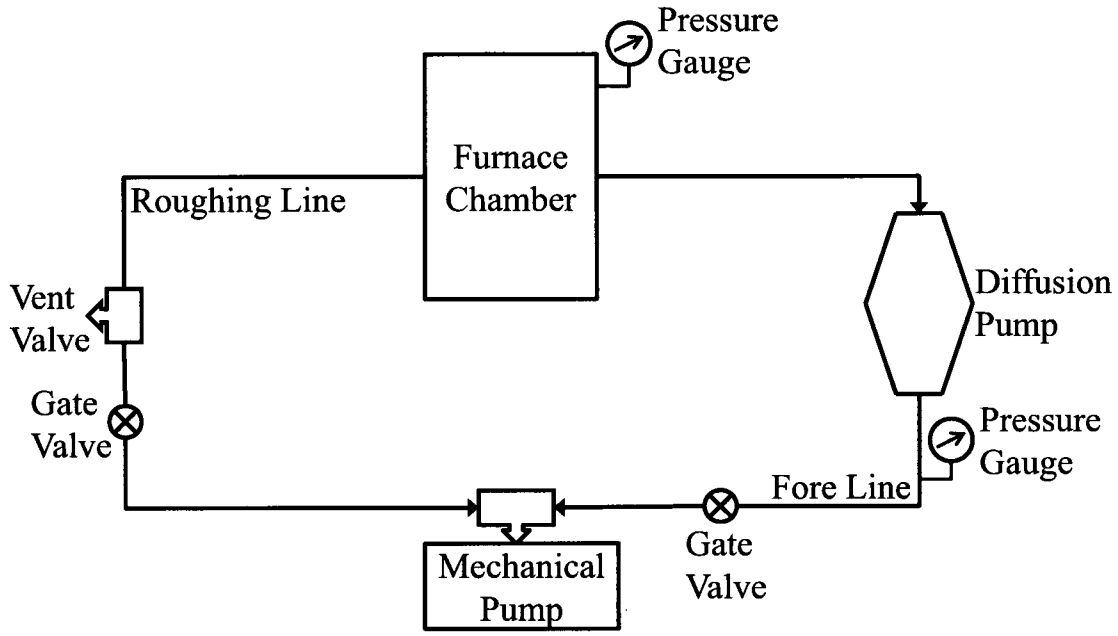

Figure 3.13: Schematic diagram of the vacuum system for operation of the prototype furnace.

During operation of the prototype furnace, the pressure within the vacuum chamber was measured using a hot cathode ion gauge for pressures less than 10^{-3} Torr. A thermocouple gauge was used to monitor pressures greater than 10^{-3} Torr. A thermocouple gauge was also mounted on the fore line of the diffusion pump to monitor the foreline pressure.

3.4 Thermometry

During operation of a furnace, it is critical to know the temperature of the interior to ensure that the desired environment is present. One C-type thermocouple (Omega Engineering Inc.) with a molybdenum sheath was introduced into the hot zone of the prototype furnace. This thermocouple was inserted into the furnace using a custom vacuum feed-through fabricated at NSCL. The thermocouple was connected to a thermocouple reader (Omega Engineering Inc.) on the atmospheric side of the furnace, and the temperatures were recorded at 4 samples per second for the duration of the tests.

Three K-type thermocouples were also used to monitor the temperature from the atmospheric side. The parts that were being monitored were the water cooled section of the thermocouple feed-through, the water cooled section of the 20.3×10^{-2} m elbow connecting the furnace chamber and the diffusion pump, and a thermocouple on the fore line of the diffusion pump. These temperatures were monitored and recorded using a custom data acquisition program in LabVIEW.

3.5 Results

This section presents measurements of temperature, pressure, and power from a test and compares the measurements with the calculated temperature and power.

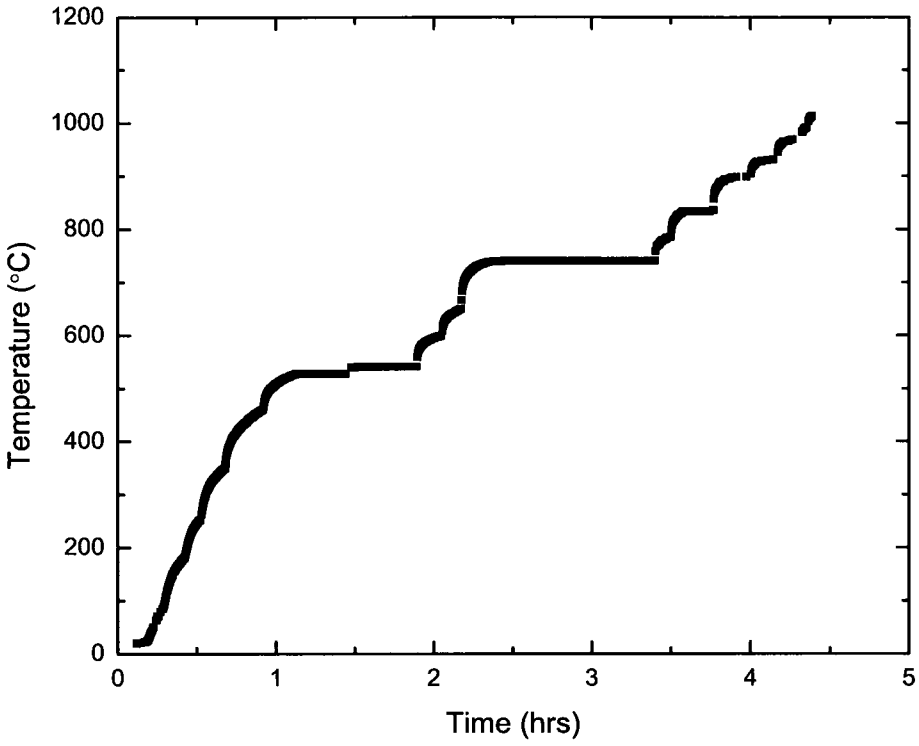

Figure 3.14: Temperature profile for a test firing of the prototype furnace.

The temperature history during the test is plotted in Figure 3.14. The temperature increased quickly in response to changes in power and remained constant when the power was unchanged. The temperature readily reached 1000 °C and the test was stopped when the copper melted. The pressure profile as a function of temperature during operation is plotted in Figure 3.15. The vacuum pump was able to maintain the pressure at less than 10^{-5} Torr until the temperature exceeds about 740 °C, at which point there was rapid formation of copper vapor.

Estimates for the resistance of tungsten wire with respect to temperature calculated from current and voltage measurements is compared with that obtained from empirically tabulated values of the resistivity of tungsten as a function of tempera-

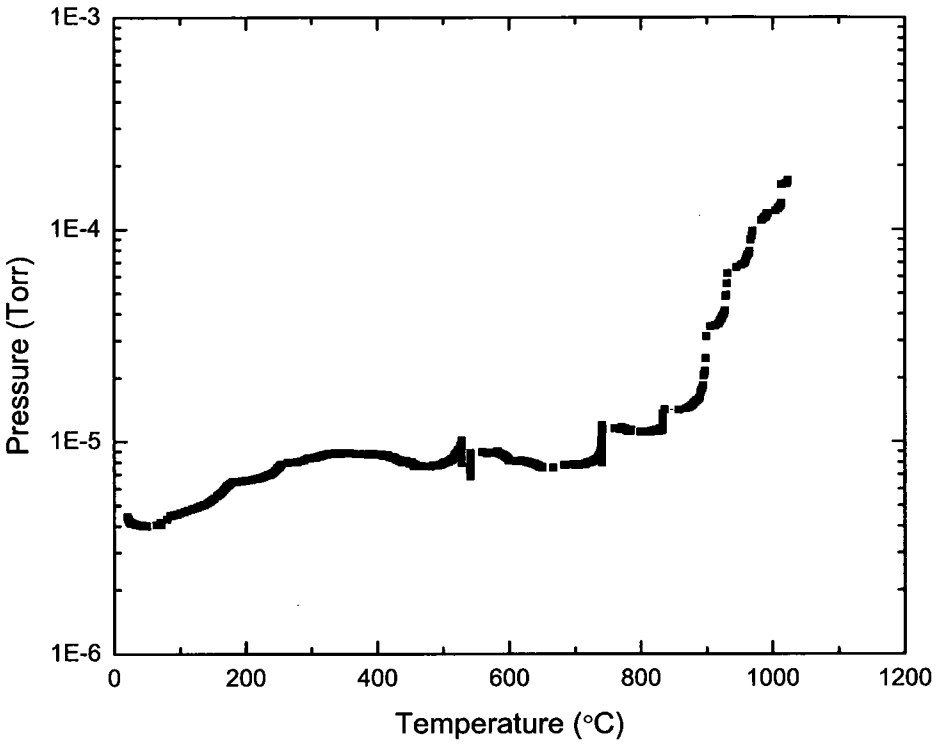

Figure 3.15: Pressure history for a test of the prototype furnace.

ture [20] and thermal expansion of the metal. Figure 3.16 compares measured and calculated values of tungsten resistance as a function of temperature.

As mentioned previously, the current and voltage input into the prototype furnace was measured using two Hewlett-Packard 34401a multimeters. The power consumed by the prototype furnace was determined as

$$P_{meas} = VI = I^2R \tag{3.16}$$

According to the conservation of energy, the electrical power consumed by the furnace should equal the losses of the furnace, which would be losses from the hot zone of the furnace to the surrounding atmosphere due to thermal radiation between shields and

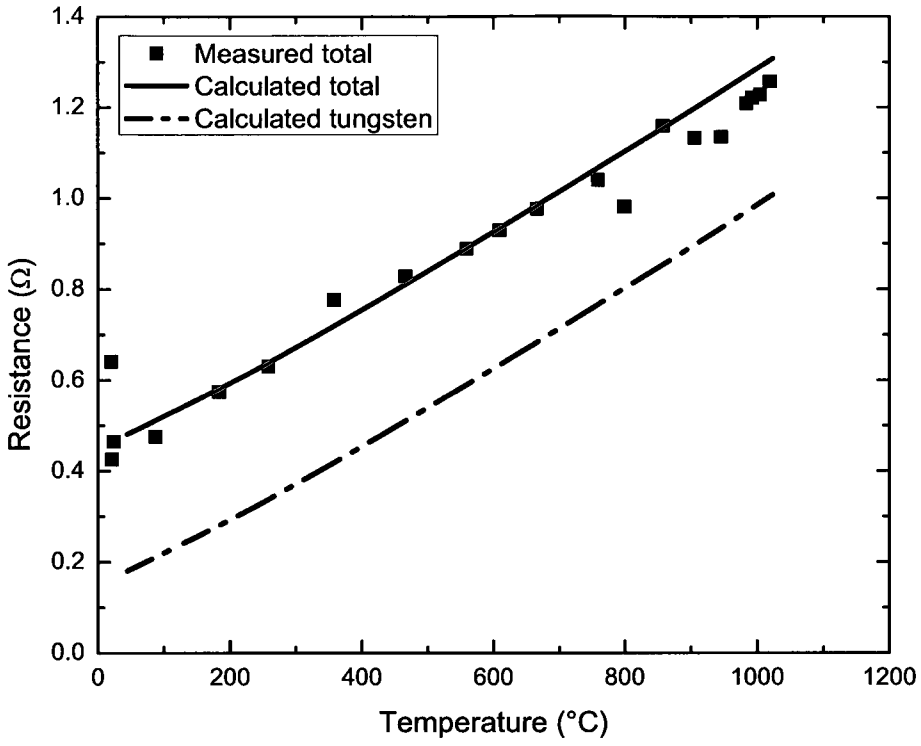

Figure 3.16: Measured total resistance and calculated total resistance for the electrical system during the test of the prototype furnace. The total resistance includes the tungsten coil resistance and the resistance of the atmospheric side wiring.

conduction of heat through the stainless steel bolts and alumina (ceramic) supports. The measured and calculated power consumption are plotted in Figure 3.17. During the test of the furnace, a steep increase in the pressure was noted when temperature approached 900 °C. This increase in pressure was attributed to the vaporization of a section of the copper target cylinder due to shorting of the tungsten heating element by contact with the surrounding copper target cylinder. The contact was associated with the sagging of the coil due to improper supports, and due to distortion of the shape of the copper cylinder at the high temperature. Figures 3.18, 3.19, and 3.20 show the damage caused due to the sagging and contact of the tungsten with

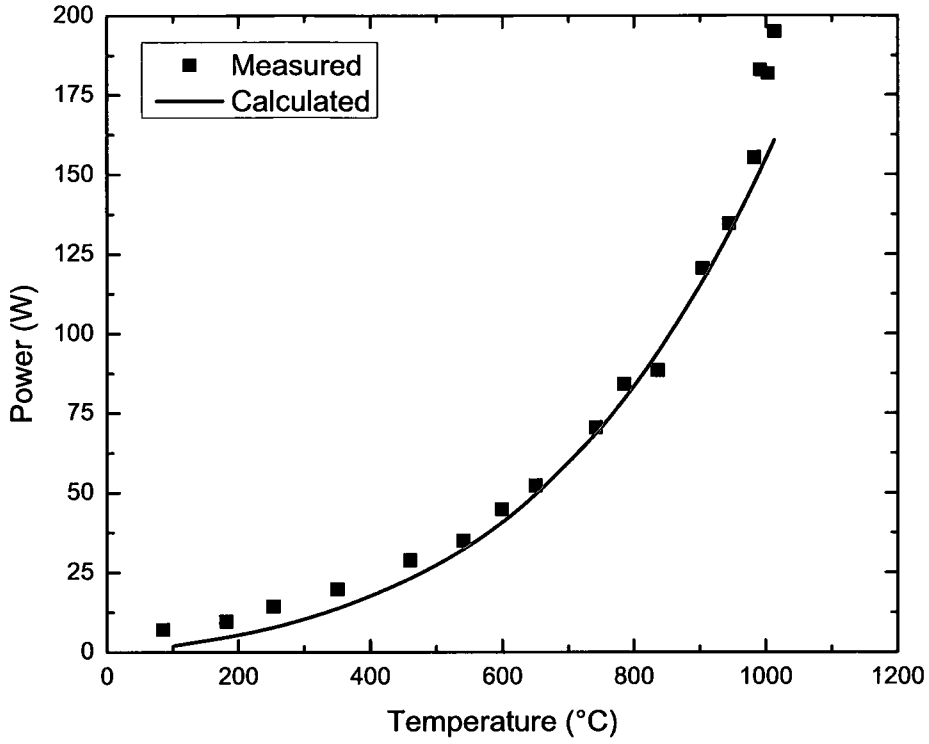

Figure 3.17: Measured and calculated power as a function of temperature for a test of the prototype furnace.

the distorted copper target cylinder. The thinning (hence increase in resistance) of the tungsten coil during vaporization after contact with the copper explains the disagreement in the calculated and experimental power values above 900 °C.

Figure 3.18: Photograph of the radiation shields after the 1000 °C test of the prototype furnace. The distortion in the shape of the target copper cylinder (at the center) in comparison with the before test condition in Figure 3.10 is clearly visible.

Figure 3.19: Close-up photograph of the hot-zone after the 1000 °C test. The location of contact of the tungsten heating coil with the distorted copper cylinder can be seen in the center.

Figure 3.20: Photograph of the tungsten heating coil after the second test of the furnace. Sagging of the coil is seen, with accumulation of windings at the bottom due to gravity. The arrow shows the location of contact with the copper cylinder due to the sagging of the coil and distortion of the shape of the copper cylinder.

3.6 Summary

A prototype furnace was fabricated using readily available materials as a proof of concept of the design of the furnace. The calculated and measured values of power agreed with each other with an average error of 5 % between the calculated and measured values between 600 and 990 °C. The discrepancy between the calculated and measured power at temperatures cooler than 600 °C was an average of 36 %, which could be associated to a 5 fold contribution (ratio of contribution of convection at 500 °C and 1000 °C) of convection at the lower temperatures in comparison with radiation. The pressure obtained during the test was less than 10^{-5} Torr for the maximum length of the test, with a significant increase due to the contact of the tungsten coil with the copper target cylinder and the subsequent vaporization of the copper target cylinder. Predicted values of the temperature dependent resistance of the tungsten wire, derived from documented values of the temperature dependent resistivity and thermal expansion of tungsten, were in good agreement with the experimental values of the resistance of the electrical circuit.

Chapter 4

Niobium Heat Treating Furnace

This chapter describes construction of a furnace to heat treat niobium samples at temperatures ranging from 100 °C to 1250 °C and pressures as low as 10^{-6} Torr. This furnace also serves as a model for a larger furnace to anneal full-sized cavities. The design for the sample treating furnace can be scaled to meet the requirements of the full size cavity heat treating furnace.

The steel vessel in Figure 3.1 from the prototype furnace was reused as the outer shell for the sample heat treating furnace. The systems involved in this furnace are similar to those in the prototype, although they are more refined, including the addition of an automated temperature controller and substitution of a turbomolecular vacuum pump for the diffusion pump used in the prototype.

4.1 Electrical system

The electrical system was upgraded to accommodate larger current and voltage as compared to the prototype, as well as higher operating temperatures for the various parts. Two single-conductor copper vacuum feed-throughs mounted on conflat flanges were used to conduct electricity from the atmospheric side of the furnace to the

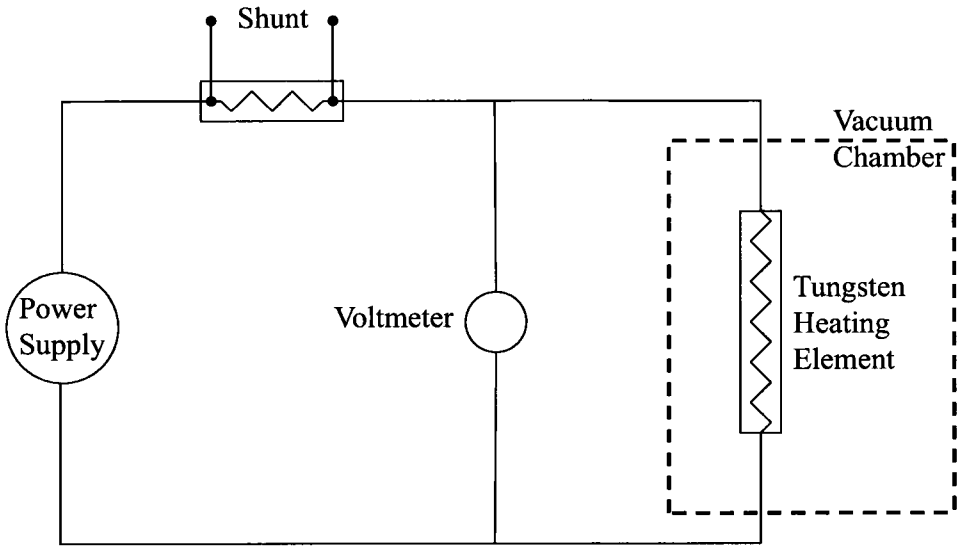

Figure 4.1: Circuit diagram of the electrical system used in the niobium sample heat treating furnace. A 2 mΩ shunt in series with the heating element was used to measure current.

vacuum side. The feed-throughs were rated for 5000 V and 30 A. A circuit diagram for the electrical system is illustrated in Figure 4.1. The shunt resistor (2 mΩ) is used to measure the current.

4.1.1 Forming the heating element

Tungsten wire of diameter 7.62×10^{-4} m was used to fabricate the heating element. Techniques adopted during coil winding were in accordance with the various conditions mentioned in Section 3.1.3, with a custom made fixture being used to wind the tungsten wire. Ceramic tubes of outer diameter 51.9×10^{-4} m and inner diameter 7.93×10^{-4} m were used to support the formed coil in place. Tungsten wire of diameter 7.62×10^{-4} m was inserted into the ceramic tubes to prevent the tubes from cracking during assembly, and to prevent the collapse of the coil in the event of

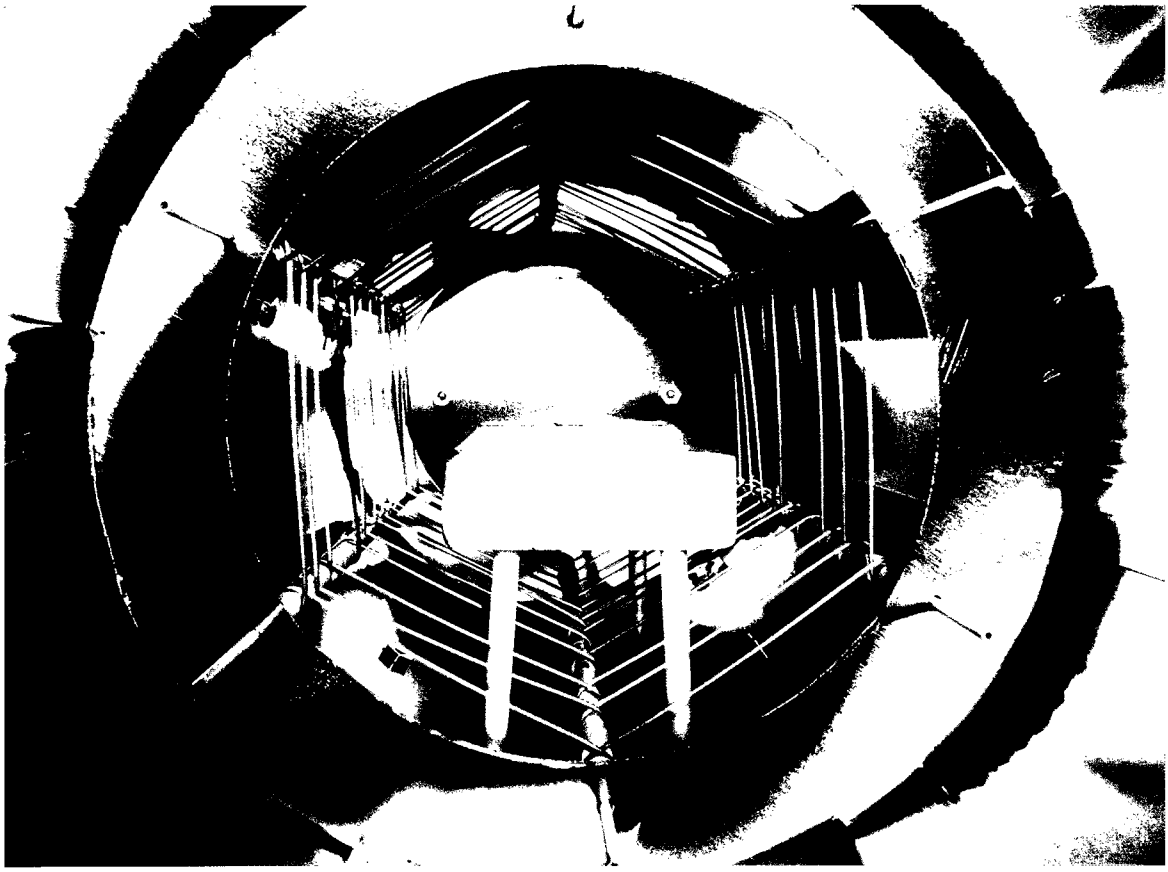

Figure 4.2: Photograph of the tungsten heating coil on ceramic support tubes within the molybdenum shields. Ceramic spacers separate the windings of the tungsten coil. Also visible is the ceramic bed for placing niobium samples for heat treatment.

accidental damage to the ceramic tubes during loading or unloading of the furnace. Ceramic spacers of custom length were made by cutting ceramic tubes of outer diameter 47.6×10^{-4} m and inner diameter 23.8×10^{-4} m using a diamond wafering blade. The ceramic spacers slid over the ceramic support tubes and were placed between the windings to prevent the coil from shorting with itself. The coil on its ceramic supports placed within the thermal shields is pictured in Figure 4.2.

The length of wire used for the coil was 4.85 m, determined by calculations similar to those described in Section 3.1.3. The calculated resistance of the coil at 27 °C, 100 °C and 1250 °C was 0.60 Ω, 0.79 Ω and 4.40 Ω, respectively.

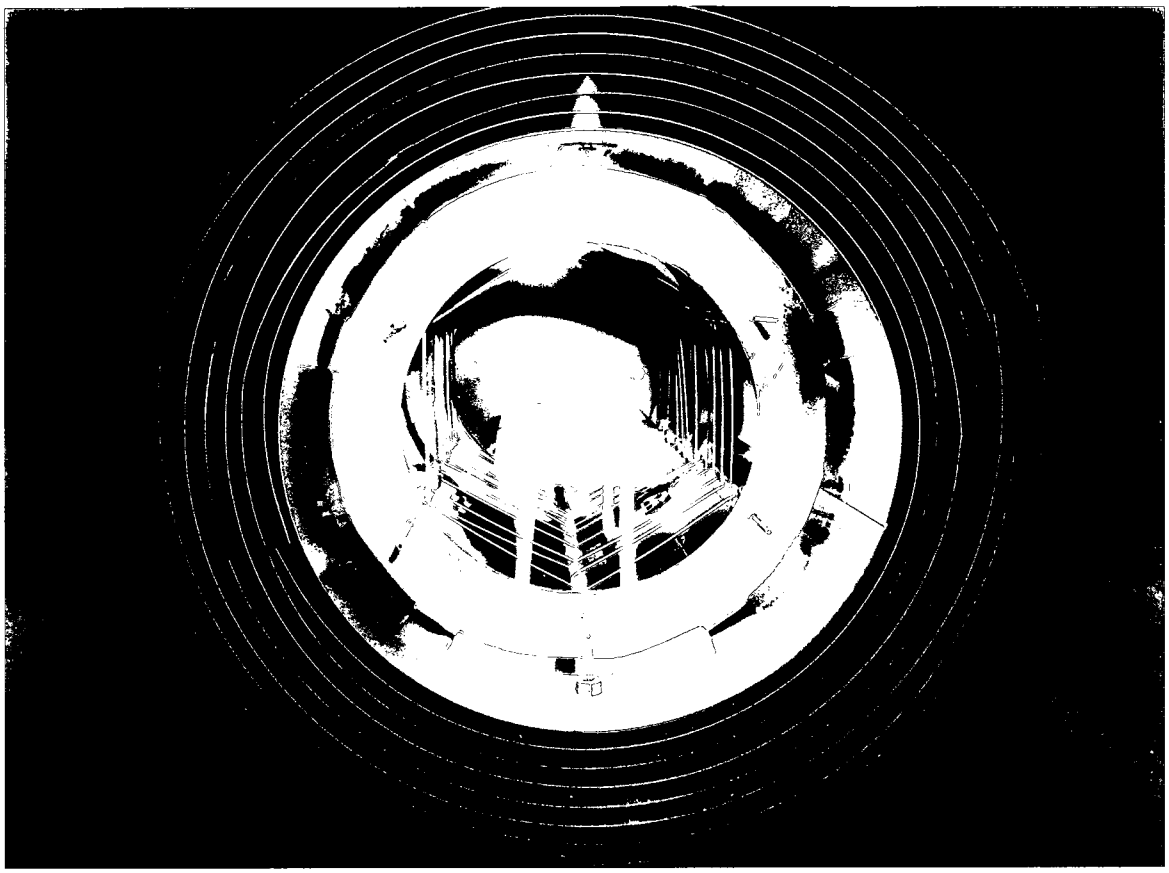

Figure 4.3: Photograph of the assembled molybdenum shields inside the vacuum vessel. The ceramic bed for placing niobium samples for heat treatment and the tungsten heating coil are also visible.

4.2 Thermal shields

Using information from Table 3.1 and Figure 3.3, molybdenum was chosen as the material for the fabrication of the thermal shields. Molybdenum sheets of thickness 2.54×10^{-4} m were cut to desired dimensions and rolled to form eight concentric cylindrical shields. The shields were attached to each other using molybdenum threaded rods, one set of the rods (length 14.6×10^{-3} m) penetrating through shields 1 through 4, and a second set (length 17.8×10^{-3} m) penetrating through shields 4 through 8. Molybdenum nuts were placed at the two ends of the threaded rod to hold the rod in place. The assembled shields are pictured in Figure 4.3.

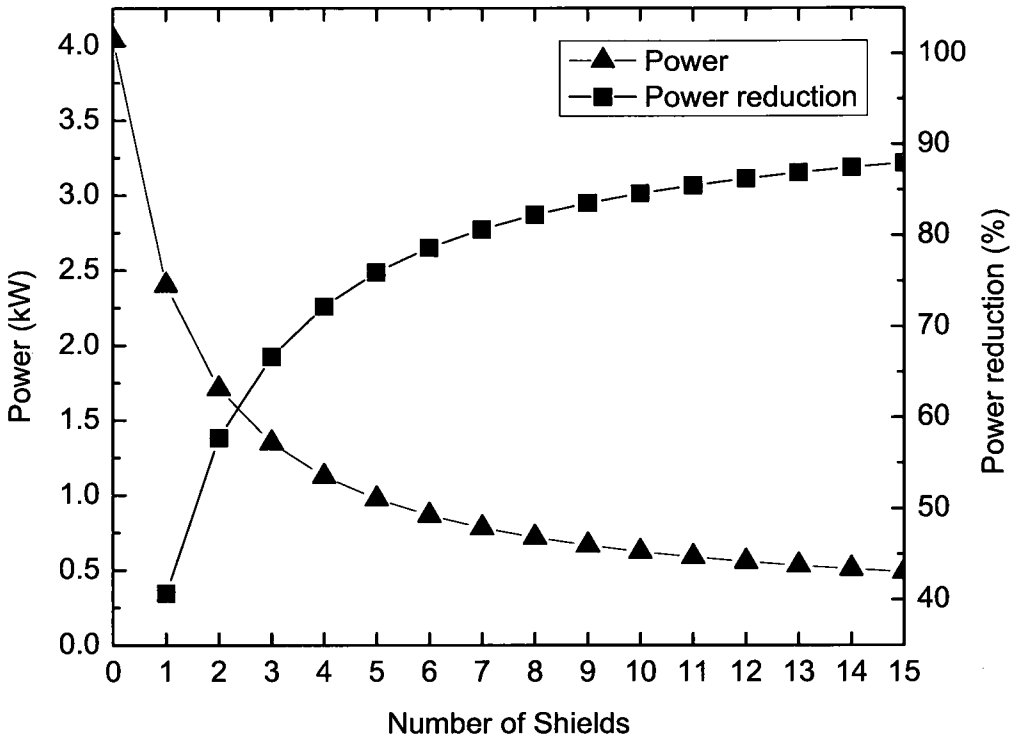

Figure 4.4: Estimated power consumption as a function of the number of radiation shields for the heat treatment furnace, for a hot-zone temperature of 1250 °C. Reduction of power consumption by the addition of each shield in comparison to the zero shields case is plotted on the right ordinate.

Radiation heat losses in the furnace were calculated as described in Section 3.2.1. The reduction in radiation losses by adding radiation shields in the vacuum furnace is shown in Figure 4.4. Despite the reduction in losses with each additional shield, there is a diminishing return for each additional shield, amounting to less than 1.5% improvement per shield for adding shields beyond nine.

Conduction losses through the molybdenum threaded rods were calculated using a resistance network, as illustrated in Figure 4.5. The two offset groups of rods were used to reduce the conduction losses by increasing the resistance to conduction for the rods as compared to the single through bolt approach in the prototype furnace.

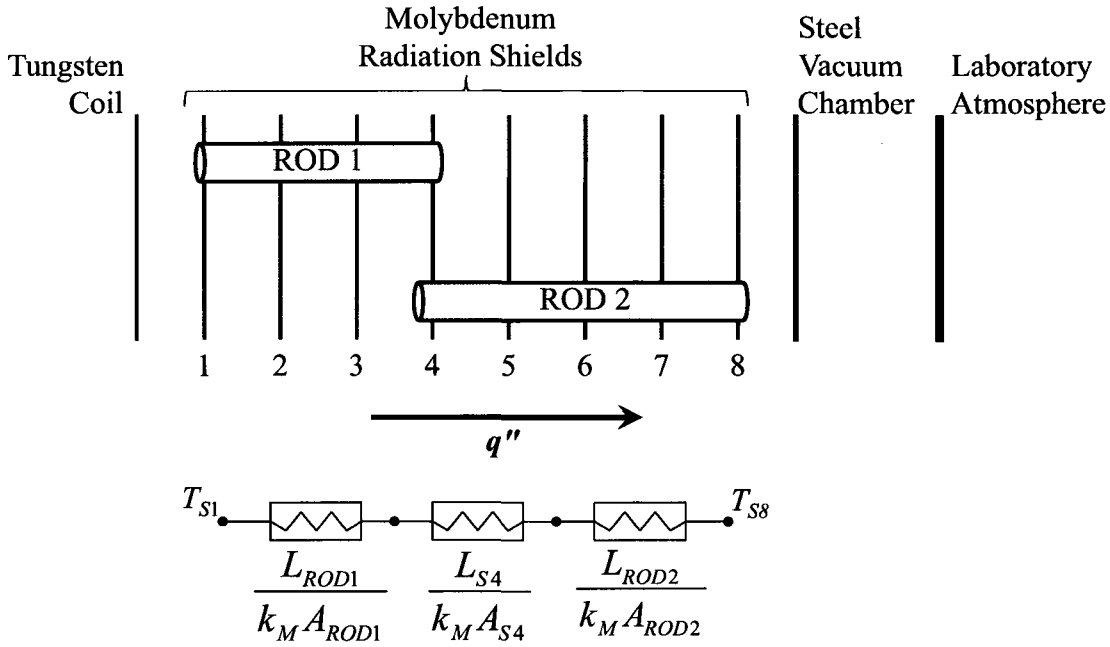

Figure 4.5: Schematic diagram of the two molybdenum rods approach for structural support of the radiation shields. Rod 1 penetrates shields 1 through 4 and is of length 14.61×10^{-3} m ($0.575''$), and rod 2 penetrates shields 4 through 8 and is of length 17.78×10^{-3} m ($0.7''$). The resistance network for conduction losses through the molybdenum rods is also shown. T_{S1} and T_{S8} are the absolute temperatures of shields 1 and 8, respectively, L_{ROD1} the length of the molybdenum rod penetrating shields 1 through 4, L_{ROD2} the length of the molybdenum rod penetrating through shields 4 through 8, L_{S4} the distance between rods 1 and 2 on shield 4, k_M the thermal conductivity of molybdenum, A_{ROD1} the cross sectional area of molybdenum rod 1, A_{ROD2} the cross sectional area of molybdenum rod 2, and A_{S4} the cross sectional area of shield 4 between rods 1 and 2.

To further reduce heat losses by conduction, custom-cut ceramic tubular spacers were inserted around the threaded rods between shields, instead of the metal nuts used for the prototype. The two offset groups of rods reduced conduction losses to 3 % of the losses with a single bolt. Provisions were made in the shields to allow thermocouples to be inserted into the heating zone, and for the leads of the heating coil to be connected to the vacuum feed-through.

4.3 Vacuum system

The vacuum system is similar to that of the prototype, with the exception of the diffusion pump being replaced with a turbomolecular pump (Alcatel). Unlike the diffusion pump, the turbomolecular pump has no oil reservoir. This reduces the possibility of reverse flow of oil vapors from the vacuum pump into the heating chamber. Similar to the diffusion pump for the prototype, the turbomolecular pump is backed with an oil sealed mechanical pump. A schematic diagram of the vacuum system is illustrated in Figure 4.6. The three valves in the vacuum system were each actuated by a pneumatic solenoid (Humphrey Products Company); model 310 was used for the roughing line and fore line valves, and model 410-39 was used for the gate valve between the turbomolecular pump and the furnace vacuum chamber.

The pressure in the vacuum chamber is measured using a thermocouple gauge for pressures greater than 10^{-3} Torr and a hot cathode ion gauge for pressures less than 10^{-3} Torr. A thermocouple pressure gauge is also mounted on the fore line of the turbomolecular pump to monitor the fore line pressure.

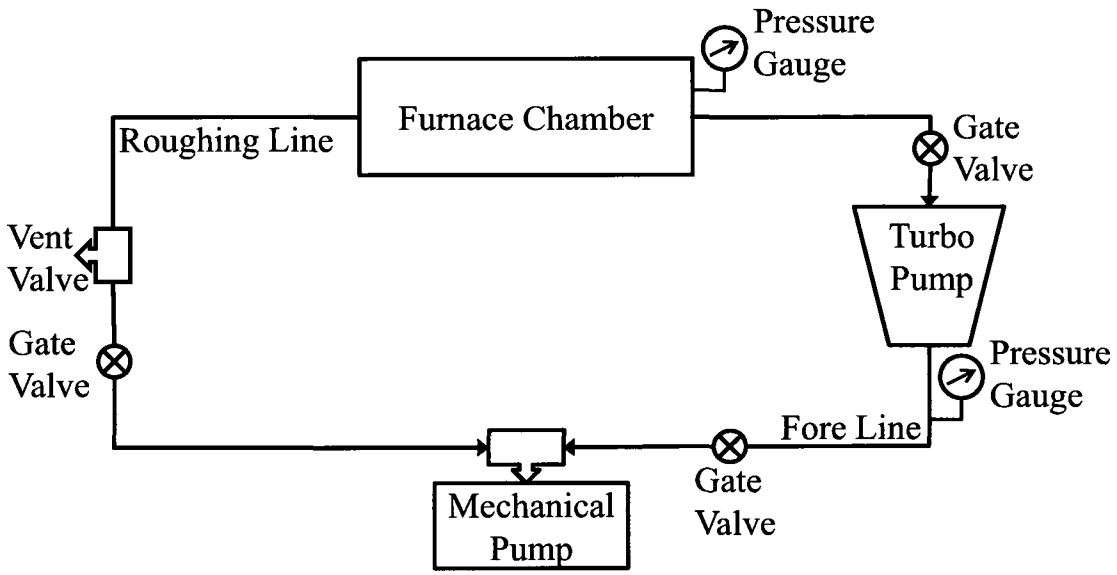

Figure 4.6: Schematic diagram of the vacuum system for the niobium sample heat treating furnace.

4.4 Thermometry

Temperatures within the hot zone are measured using two bare wire C-type thermocouples (Omega Engineering Inc.) rated for use up to 2300 °C. One K-type thermocouple (Omega Engineering Inc.) is employed to monitor the temperature of shield number 4. Two K-type thermocouples (Omega Engineering Inc.) are mounted on the atmospheric surface of the vacuum chamber to monitor temperatures near the thermocouple gauge feed-through and at the bottom of the vacuum chamber. A J-type thermocouple (Omega Engineering Inc.) is attached to the outside of the turbomolecular pump to monitor its temperature to prevent over-heating during operation of the furnace. The two C-type and the K-type thermocouple within the vacuum chamber were mounted through two 3-pair thermocouple vacuum feed-throughs (Insulator Seal) which were mounted on conflat flanges, one each for the C-type and K-type thermocouples.

4.5 Data acquisition

A LabVIEW program was written to monitor and control the various parameters associated with the operation of the heat treating furnace. The thermocouples were monitored using two 4 channel, ± 0.08 V, 14 samples per second, 24 bit thermocouple differential analog input modules (National Instruments, model NI 9211). The pneumatic solenoid actuators for the valves were controlled through an 8 channel, 24 V, sourcing digital output module (National Instruments, model NI 9472). A 2 mΩ shunt was used to monitor the current in the circuit, and the signal from the shunt was amplified using a DATAFORTH SCM5B30-02 ± 50 mV to ± 5 V signal amplifier.

4.6 Results

The temperature history of the thermocouples within the furnace hot zone and on the vacuum vessel during an initial run of the furnace are plotted in Figure 4.7. The temperature increased quickly in response to changes in power and remained constant when the power was unchanged. The temperature readily reached 1250 °C. The temperature and pressure profiles during operation are compared in Figure 4.8. The vacuum pump was able to maintain the pressure at less than 10^{-5} Torr for most of run. The temperature was held steady at 890 °C for two hours to facilitate the removal of volatile components and allow the vacuum pump to equalize the pressure.

The resistance of the tungsten wire calculated as a function of temperature from current and voltage measurements is compared with that obtained from empirically tabulated values of the resistivity of tungsten as a function of temperature [20] and thermal expansion of the metal. Figure 4.9 compares measured and calculated values of tungsten resistance as a function of temperature. The calculated values of resistance

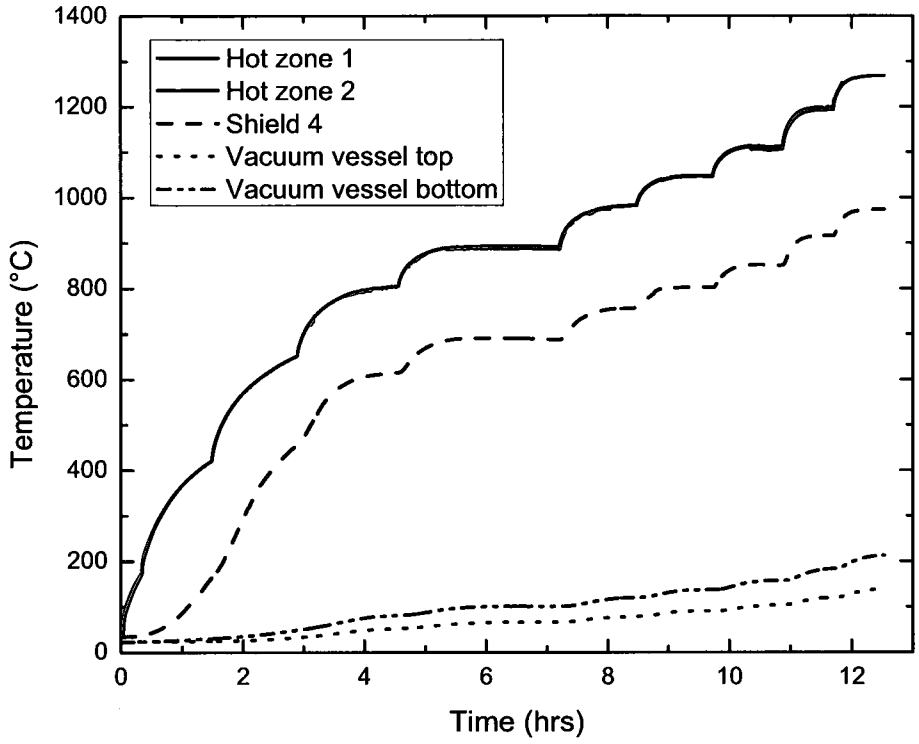

Figure 4.7: Measured temperature profiles during an initial run of the niobium sample heat treating furnace. Temperatures in the hot-zone were measured with two C-type thermocouples; other temperatures were measured with K-type thermocouples. The temperatures at the two locations in the hot zone, 1 and 2, substantially overlap.

agree within 3 % with the measured values above 600 °C, and have a discrepancy of 7 % across the entire measured temperature range. The measured and calculated power consumption are plotted in Figure 4.10. The calculated estimates for power consumption agree within 5 % with the measured values.

The temperatures measured by the thermocouples within the hot zone were verified using disks made from materials that exhibit controlled shrinkage over a period of time at a given temperature (TempTabs). Two sets of these disks were used, one set (TempTab 300) calibrated for temperatures between 800 and 1150 °C, and the other set (TempTab 600) calibrated for temperatures between 1100 and 1300 °C. Three

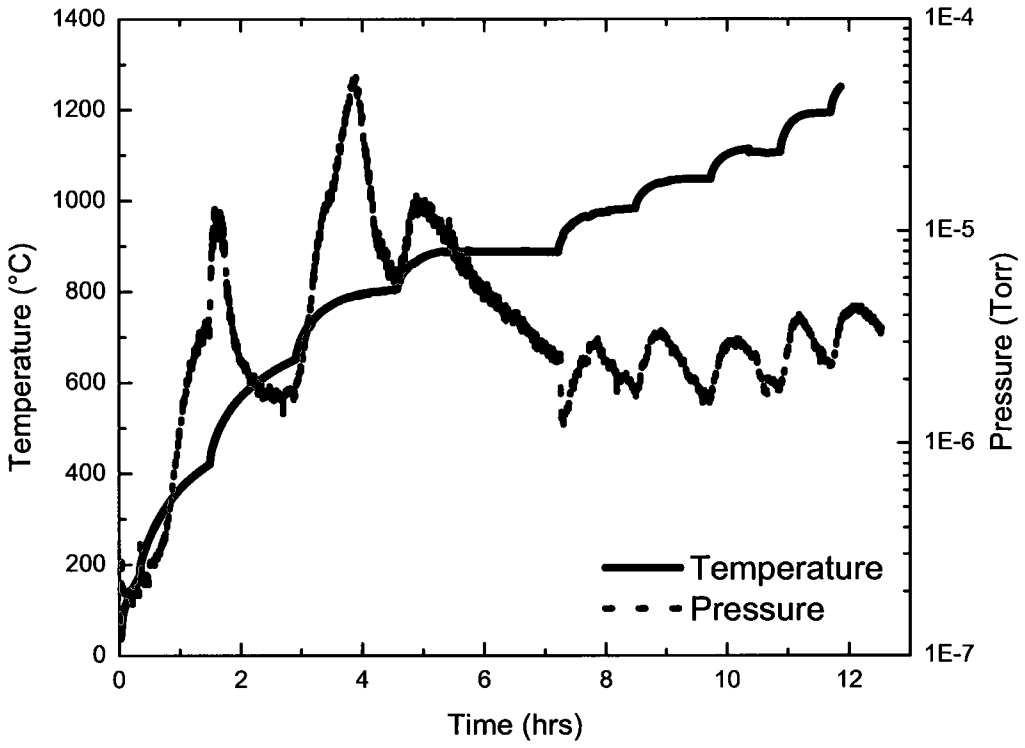

Figure 4.8: Temperature and pressure histories during a run of the furnace. Between hours 5 and 7 the furnace is set to maintain 890 °C for a soak, that is, to allow volatile components to be pumped out, causing the pressure to drop. Subsequent increases in temperature are met with small transient pressure changes.

rows of TempTabs, spanning the length of the ceramic sample bed, were subjected to a test up to 900 °C. Each row had seven TempTabs spanning the width of the sample bed, alternating with a TempTab 600 and a TempTab 300. The three rows of TempTabs on the sample bed before the test are pictured in Figure 4.11. The redundant TempTabs on the sample bed were used to determine the temperature distribution within the furnace. This was done during a test when the temperature was maintained at 920 °C for 30 minutes. The measured dimensions of the TempTabs after the test demonstrated that the temperature distribution around the ceramic sample bed is within ± 5 °C.

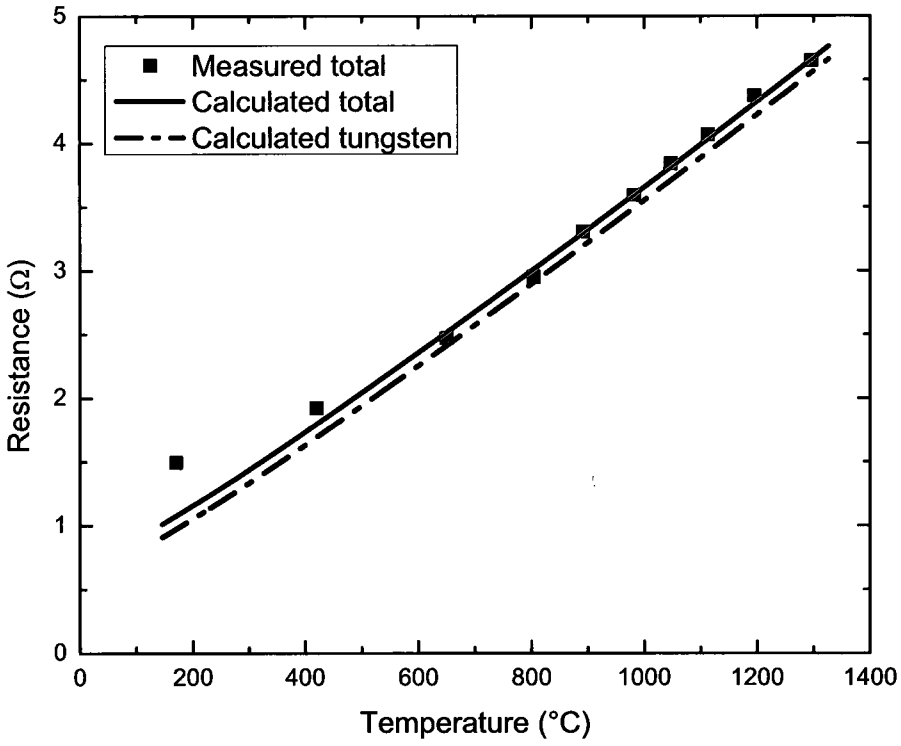

Figure 4.9: Measured total resistance and calculated total resistance for the electrical system during the test operation of the niobium sample heat treating furnace. The total resistance includes the tungsten coil resistance and the resistance of the wiring on the atmospheric side.

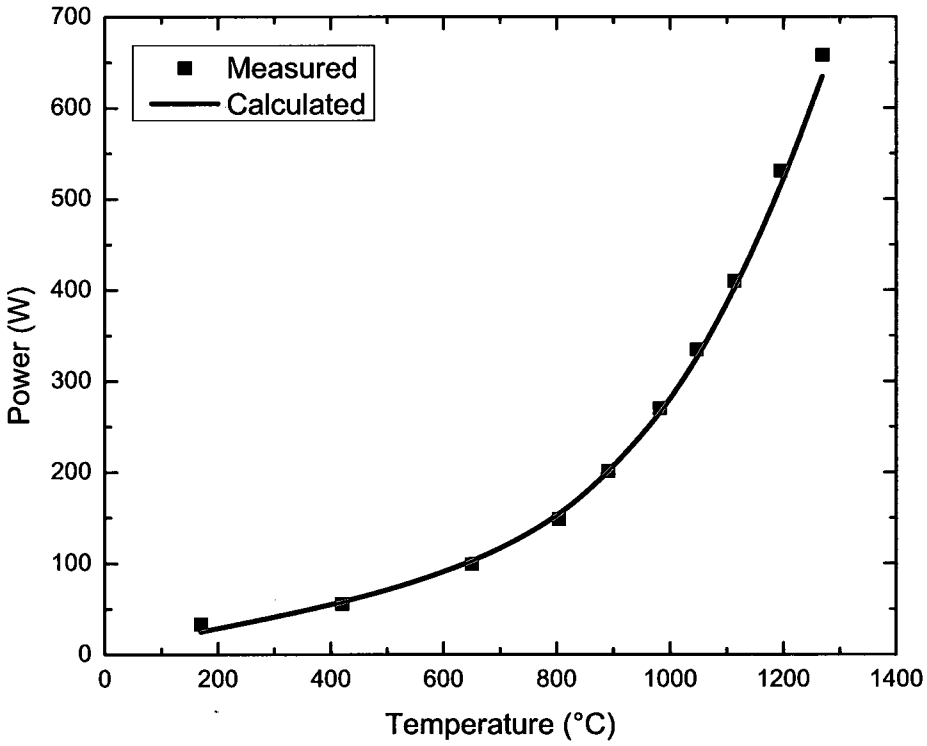

Figure 4.10: Measured and calculated power as a function of temperature for a test of the niobium sample heat treating furnace.

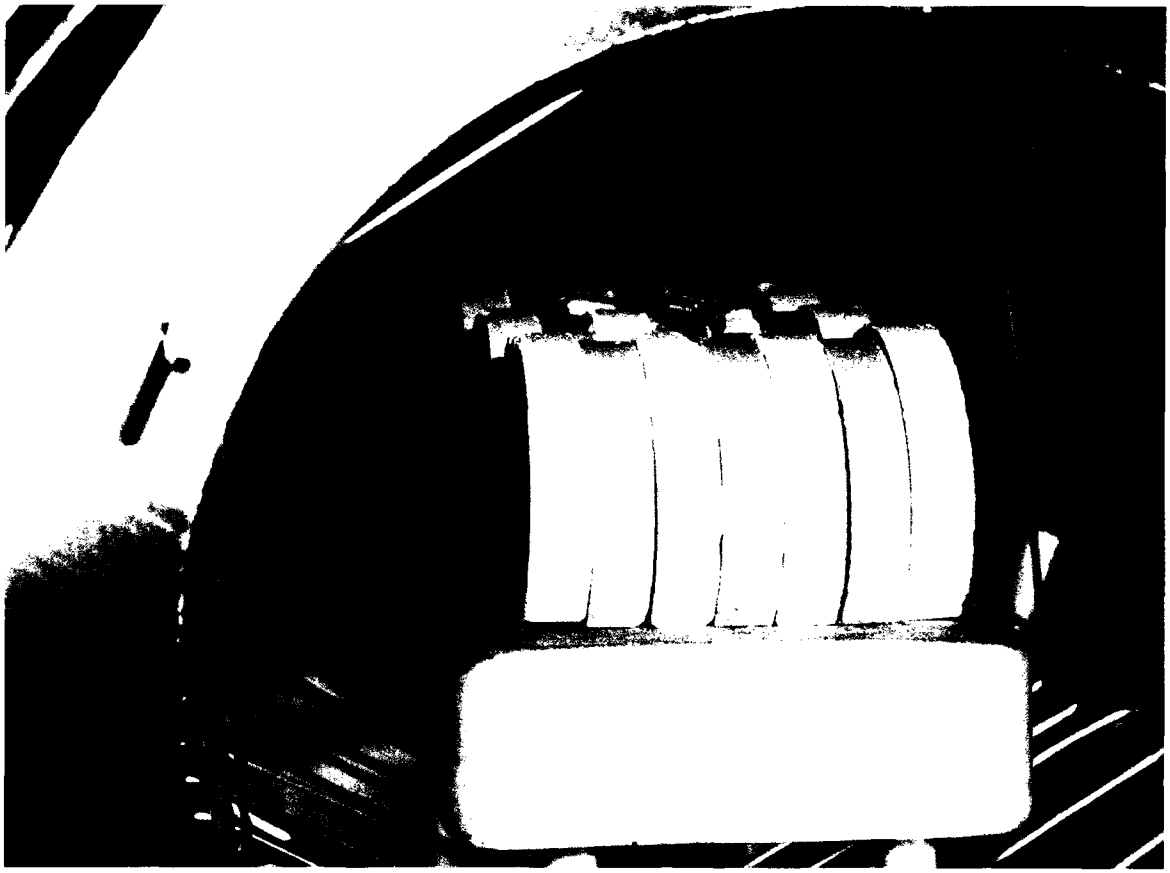

Figure 4.11: Photograph of the three rows of TempTabs used to verify the thermocouple measurements, and to check the temperature distribution within the hot zone of the niobium sample heat treating furnace. Each row contains seven TempTabs, alternating between TempTab 600 (1100 °C – 1300 °C) and TempTab 300 (800 °C – 1150 °C). The three rows span the length of the ceramic sample bed, and each row spans the width of the bed.

4.7 Conclusion

A high-temperature, high-vacuum furnace was fabricated to heat treat niobium samples at temperatures ranging from 100 °C to 1250 °C. The calculated and measured values of the power required for the tungsten heating element agreed with each other with an average discrepancy of 5 %. The pressure measured during the test was less than 10^{-5} Torr for the maximum length of the test. A longer hold time at 600 °C might have enabled the pump to remove more of the volatile components and maintain the pressure below 5×10^{-6} Torr through the entire length of the test. Predicted values of the temperature dependent resistance of the tungsten wire, derived from documented values of the temperature dependent resistivity and thermal expansion of tungsten, were in good agreement with the experimental values of the resistance of the electrical circuit.

The ceramic sample bed installed in the sample heat treating furnace can accommodate four of the largest samples (largest dimensions of 8 cm × 2 cm × 0.3 cm) used for heat transfer research placed flat on the 8 cm × 2 cm sides simultaneously. If placed on their 8 cm × 0.3 cm sides, sixteen samples can be accommodated along with 0.3 cm ceramic spacers between the samples. Materials research samples are of smaller dimensions, hence larger quantities can be heat treated simultaneously. Pumping the system to pressures as low as 10^{-6} Torr takes approximately 2 hours. The furnace requires approximately 18 hours to cool to room temperature from 1250 °C. Hence, depending on the desired ramp rate and time at the heat treating temperature, a minimum of four niobium samples can be heat treated within 36 – 48 hours.

A furnace to heat treat niobium cavities would require a tungsten heater of diameter approximately 0.508 m (20″) and length approximately 0.762 m (30″), and eight radiation shields with diameter ranging from 0.635 m (25″) to 0.813 m (32″) in increments of 0.0254 m (1″) and lengths ranging from 0.889 m (35″) to 1.067 m (42″)

in increments of 0.0254 m (1″), and having a vacuum chamber with dimensions of diameter 0.889 m (35″) and length 1.14 m (45″). The power required for temperatures of 1250 °C and 1500 °C would be 9 kW and 18 kW, respectively. The high power requirements would necessitate water-cooled electrical feed throughs to prevent the copper from over-heating. Due to the size of the vacuum chamber, large turbomolecular vacuum pumps would be required. A roots blower between the turbomolecular pump and the mechanical roughing pump would increase the pumping speed of the pumps.

BIBLIOGRAPHY

[1] H. Padamsee, J. Knobloch, and T. Hays, *RF Superconductivity for Accelerators.* Wiley-Interscience Publication, 1998.

[2] G. Ciovati, "Effect of Low-Temperature Baking on the Radio-Frequency Properties of Niobium Superconducting Cavities for Particle Accelerators," *J. Appl. Phys.*, vol. 96, pp. 1591–1600, 2004.

[3] G. E. Dieter, *Mechanical Metallurgy.* McGraw-Hill Book Company, third ed., 1986.

[4] H. Lengeler, W. Weingarten, G. Müller, and H. Piel, "Superconducting Niobium Cavities of Improved Thermal Conductivity," *IEEE Trans. Magn.*, vol. MAG-21, pp. 1014–1017, 1985.

[5] H. Padamsee, "A New Purification Technique for Improving the Thermal Conductivity of Superconducting Nb Microwave Cavities," *IEEE Trans. Magn.*, vol. MAG-21, pp. 1007–1010, 1985.

[6] P. Kneisel, "Use of the titanium solid state gettering process for the improvement of the performance of superconducting rf cavities," *J. Less-Common Met.*, vol. 139, pp. 179–188, 1988.

[7] B. Aune, R. Bandelmann, D. Bloess, B. Bonin, A. Bosotti, M. Champion, C. Crawford, G. Deppe, B. Dwersteg, D. A. Edwards, H. T. Edwards, M. Ferrario, M. Fouaidy, P.-D. Gall, A. Gamp, A. Gössel, J. Graber, D. Hubert, M. Hüning, M. Juillard, T. Junquera, H. Kaiser, G. Kreps, M. Kuchnir, R. Lange, M. Leenen, and M. Liepe, "Superconducting TESLA cavities," *Phys. Rev. ST Accel. Beams*, vol. 3, no. 9, 2000.

[8] B. Visentin, J. P. Charrier, B. Coadou, and D. Roudier, "Cavity Baking: A Cure for the High Accelerator Field Q_0 Drop," *Proc.* 9^{th} *Workshop on RF Supercond.*, 1999.

[9] G. Müller and H. Padamsee, "High Temperature Annealing of Superconducting Cavities Fabricated from High Purity Niobium," *IEEE Part. Acc. Conf.*, pp. 1833–1835, 1987.

[10] A. Aizaz, T. L. Grimm, and N. T. Wright, "Thermal design studies of niobium SRF cavities," *Proc. SRF-2007*, pp. 362–366, 2007.

[11] H. Safa, D. Moffat, B. Bonin, and F. Koechlin, "Advances in the Purification of Niobium by Solid State Gettering with Titanium," *J. Alloy Compd.*, vol. 232, pp. 281–288, 1996.

[12] H. Safa, D. Moffat, F. Koechlin, E. Jacques, and Y. Boudigou, "Nb Purification by Ti Gettering," *Proc. 7^{th} Workshop on RF Supercond.*, vol. 2, pp. 649–652, 1995.

[13] A. Brinkmann, D. Hui, H. Kaiser, D. Proch, W. Singer, and X. Singer, "Quality Control and Purification Heat Treatment of Niobium for TTF," *Proc. 9^{th} Workshop on RF Supercond.*, 1999.

[14] S. K. Chandrasekaran, J. V. Beck, T. R. Bieler, C. C. Compton, and N. T. Wright, "Parameter Estimation of the Thermal Conductivity of Superconducting Niobium," *Therm. Cond.*, vol. 30, In Press.

[15] T. R. Bieler, N. T. Wright, F. Pourboghrat, C. Compton, K. T. Hartwig, D. Baars, A. Zamiri, S. K. Chandrasekaran, P. Darbandi, H. Jiang, E. Skoug, S. Balachandran, G. E. Ice, and W. Liu, "Physical and mechanical metallurgy of high purity Nb for accelerator cavities," *Phys. Rev. ST Accel. Beams*, vol. 13, no. 10, 2010.

[16] S. K. Chandrasekaran, D. Baars, C. Compton, T. Bieler, and N. T. Wright, "Measurement of the Thermal Conductivity of Large Grain Niobium for SRF Cavities." SRF Materials Workshop, NSCL, East Lansing, MI, October 2008.

[17] A. Aizaz, P. Bauer, T. L. Grimm, N. T. Wright, and C. Z. Antoine, "Measurements of Thermal Conductivity and Kapitza Conductance of Niobium for SRF Cavities for Various Treatments," *IEEE T. Appl. Supercon.*, vol. 17, pp. 1310–1313, 2007.

[18] W. Singer, A. Brinkmann, A. Ermakov, J. Iversen, G. Kreps, A. Matheisen, D. Proch, D. Reschke, X. Singer, M. Spiwek, H. Wen, and H. G. Brokmeier, "Large Grain Superconducting RF Cavities at DESY," *Proc. LINAC-2006*, 2006.

[19] *Research Chemicals, Metals and Materials Catalog.* Alfa Aesar®, 2008-09.

[20] D. R. Lide, ed., *CRC Handbook of Chemistry and Physics.* CRC Press, 89^{th} ed., 2008-09.

[21] C. J. Smithells, ed., *Metals Reference Book.* Butterworth & Co. Ltd., 1976.

[22] D. R. Lide, ed., *CRC Handbook of Chemistry and Physics.* CRC Press, 76$^{\text{th}}$ ed., 1995-96.

[23] F. Rosebury, *Handbook of Electron Tube and Vacuum Techniques.* American Institute of Physics, 1993.

[24] F. P. Incropera and D. P. DeWitt, *Introduction to Heat Transfer.* John Wiley and Sons, fourth ed., 2002.

[25] R. S. Graves, T. G. Kollie, D. L. McElroy, and K. E. Gilchrist, "The Thermal Conductivity of AISI 304L Stainless Steel," *Int. J. Thermophys.*, vol. 12, pp. 409–415, 1991.

[26] R. G. Munro, "Evaluated Material Properties for a Sintered α-Alumina," *J. Am. Ceram. Soc.*, vol. 80, pp. 1919–1928, 1997.